

Elucidating the coordination chemistry of the radium ion for targeted alpha therapy

Alexander S. Ivanov,^{*a} Megan E. Simms,^a Vyacheslav S. Bryantsev,^a Paul D. Benny,^b Justin R. Griswold,^b Laetitia H. Delmau,^b Nikki A. Thiele^{*a}

^a Chemical Sciences Division, Oak Ridge National Laboratory, Oak Ridge, Tennessee 37831, United States.
E-mail: thielena@ornl.gov, ivanova@ornl.gov

^b Radioisotope Science and Technology Division, Oak Ridge National Laboratory, Oak Ridge, Tennessee 37831, United States

TABLE OF CONTENTS

	<u>page</u>
1. EXPERIMENTAL PROCEDURES.....	6
1.1 Reagents.....	6
1.2 Radioisotope Quality Control and Counting.....	7
1.2.1 General.....	7
1.2.2 Gamma spectroscopy.....	7
1.2.3 Liquid scintillation counting.....	7
1.3 Protonation Constants and Non-Radioactive Complex Stabilities by Potentiometric Titration.....	9
1.4 ²²³ Ra Stability Constant Determination: Solvent Extraction Method.....	11
1.4.1 Organic phase preparation.....	11
1.4.2 Aqueous phase preparation.....	12
1.4.3 Liquid-liquid extraction.....	12
1.4.4 Results.....	12
1.5 ¹³³ Ba and ²²³ Ra Stability Constant Determination: Cation Exchange Method.....	13
1.5.1 Resin conditioning.....	13
1.5.2 Sample preparation and workup.....	14
1.5.3 Effects of metal contaminants.....	15
1.5.4 Data analysis.....	17
1.5.5 Correction of [Ra(DOTA)] ²⁻ stability constant for Na ⁺ binding.....	18
1.5.6 ¹³³ Ba distribution measurements at low pH.....	19
1.6 Density Functional Theory Calculations.....	20
2. SUPPORTING FIGURES, SCHEMES, AND TABLES.....	24
2.1 Stability Constant Determination.....	24
2.1.1 Solvent extraction method (²²³ Ra).....	24
2.1.2 Potentiometric titration (nonradioactive alkaline earths).....	25
2.1.3 Cation exchange method (²²³ Ra and ¹³³ Ba).....	29
2.2 Density Functional Theory Calculations.....	39
3. REFERENCES.....	41
4. APPENDICES.....	44
A. HPGe Gamma-Ray Spectra.....	44
B. Sample Gaussian 16 Input Files.....	46
C. Cartesian Coordinates.....	54

LIST OF TABLES

<u>Table</u>	<u>page</u>
Table S1. Protonation constants of macropa and DOTA determined at 25 °C and I = 0.2 M NaCl.....	25
Table S2. Summary of distribution ratios and ²²³ Ra complex stoichiometry obtained from cation exchange experiments with varying concentrations of macropa at p[H] 5.62, 5.92, and 6.29.....	30
Table S3. Summary of distribution ratios and ²²³ Ra complex stoichiometry obtained from cation exchange experiments with varying concentrations of DOTA at p[H] 7.68, 8.07, and 8.46.....	30
Table S4. Summary of log β _{app} values for complexation of Ra ²⁺ by DOTA or macropa as a function of solution p[H].....	36
Table S5. Comparison of experimental (ΔΔG ^{exp} _{aq}) and calculated (ΔΔG ^{calc} _{aq}) [B3LYP/SC/6-31+G* level of theory] Gibbs free energies (kcal/mol) for the reaction given by Equation (2) in the main text.....	39
Table S6. Wiberg bond indices of AE–ligand bonds in the studied complexes at the B3LYP/SC/def2TZVPP level.....	39
Table S7. Leading donor-acceptor NBO interactions and their second-order stabilization energies E ⁽²⁾ (kcal/mol) for the macropa and DOTA complexes with the alkaline-earth (AE) metal ions at the B3LYP/SC/def2TZVPP level.....	39
Table S8. Calculated relative strain energies for neutral diaza-18-crown-6 and cyclen fragments of macropa and DOTA, respectively.....	40

LIST OF FIGURES

<u>Figure</u>	<u>page</u>
Figure S1. Distribution of ^{223}Ra into HDEHP/ <i>o</i> -xylene from a buffered aqueous phase in the presence or absence of macropa as a function of pH	24
Figure S2. Overlay of potentiometric titration curves of macropa (1 mM) in the absence and presence of 1 equiv of Ca^{2+} , Sr^{2+} , or Ba^{2+}	25
Figure S3. Representative potentiometric titrations of macropa (1 mM) in the (a) absence or presence of equimolar (b) Ca^{2+} , (c) Sr^{2+} , or (d) Ba^{2+} , showing best-fit pH values calculated by Hyperquad	26
Figure S4. Overlay of potentiometric titration curves of DOTA (1 mM) in the absence and presence of 1 equiv of Ca^{2+} , Sr^{2+} , or Ba^{2+}	27
Figure S5. Representative potentiometric titrations of DOTA (1 mM) in the (a) absence or presence of equimolar (b) Ca^{2+} , (c) Sr^{2+} , or (d) Ba^{2+} , showing best-fit pH values calculated by Hyperquad.....	28
Figure S6. Overlay of potentiometric titration curves of macropa (1 mM) in 0.2 M NaCl or NMe_4Cl	28
Figure S7. Representative determination of the stoichiometry of the complex formed between Ra^{2+} and macropa from distribution data at p[H] 5.62.....	29
Figure S8. Representative determination of the stoichiometry of the complex formed between Ra^{2+} and DOTA from distribution data at p[H] 7.68	29
Figure S9. Determination of β_{app} for $[\text{Ra}(\text{macropa})]$ from distribution data at pH 12.4 and $I = 0.2 \text{ M NaOH/Cl}$	31
Figure S10. Determination of β_{app} for the Ra^{2+} complex of macropa from distribution data at p[H] 5.62.....	31
Figure S11. Determination of β_{app} for the Ra^{2+} complex of macropa from distribution data at p[H] 5.92.....	32
Figure S12. Determination of β_{app} for the Ra^{2+} complex of macropa from distribution data at p[H] 6.29.....	32
Figure S13. Determination of β_{app} for the Ra^{2+} complex of DOTA from distribution data at p[H] 7.68.....	33
Figure S14. Determination of β_{app} for the Ra^{2+} complex of DOTA from distribution data at p[H] 8.07.....	33

Figure S15. Determination of β_{app} for the Ra^{2+} complex of DOTA from distribution data at p[H] 8.46.....	34
Figure S16. Variation in β_{app} of Ra^{2+} and Ba^{2+} complexes of macropa measured at different p[H] values.....	34
Figure S17. Variation in β_{app} of Ra^{2+} and Ba^{2+} complexes of DOTA measured at different p[H] values.....	35
Figure S18. Determination of β_{app} for the Ba^{2+} complex of macropa from distribution data at p[H] 5.62.....	36
Figure S19. Determination of β_{app} for the Ba^{2+} complex of macropa from distribution data at p[H] 5.92 (n = 1).	37
Figure S20. Determination of β_{app} for the Ba^{2+} complex of DOTA from distribution data at p[H] 6.67 (n = 3)	37
Figure S21. Determination of β_{app} for the Ba^{2+} complex of DOTA from distribution data at p[H] 7.19 (n = 5)	38
Figure S22. Determination of β_{app} for the Ba^{2+} complex of DOTA from distribution data at p[H] 7.45 (n = 3)	38
Figure A1. HPGe gamma-ray spectra of ^{223}Ra used in this work	44
Figure A2. HPGe gamma-ray spectra of ^{133}Ba used in this work	45

1. EXPERIMENTAL PROCEDURES

Caution! The isotopes ^{223}Ra and ^{133}Ba are radioactive. Work should only be performed by trained personnel in facilities equipped to safely handle and store these materials.

1.1 Reagents

All solvents and reagents were of ACS grade or higher and were purchased from commercial sources. Inductively coupled plasma (ICP) standard solutions of barium, strontium, and calcium (1,000 $\mu\text{g/mL}$, BDH Aristar) in dilute nitric acid were purchased from VWR (Radnor, PA, USA). 1,4,7,10-Tetraazacyclododecane-*N,N',N'',N'''*-tetraacetic acid (DOTA, min. 98%) was purchased from Strem (Newburyport, MA, USA) and used as received. 1,7,10,16-Tetraoxa-4,13-diazacyclooctadecane was purchased from EMD Millipore (Darmstadt, Germany). Macropa $\cdot 2\text{HCl}\cdot 1.5\text{H}_2\text{O}$ was prepared according to published literature procedures¹⁻³ and recrystallized four times from 6 M HCl (Optima HCl and ultra-trace elemental analysis grade H_2O , Fisher Scientific, Pittsburgh, PA, USA) by precipitation with acetone. Macropa was analyzed by ^1H and $^{13}\text{C}\{^1\text{H}\}$ nuclear magnetic resonance (NMR) spectroscopy (AvanceIII 400 MHz spectrometer, Bruker, Billerica, MA, USA), reverse-phase C_{18} high-performance liquid chromatography (HPLC, Shimadzu, Kyoto, Japan), and elemental analysis (Atlantic Microlab, Norcross, GA, USA), and was determined to be >99.5% pure. Di-(2-ethylhexyl)phosphoric acid (HDEHP) was purchased from Alfa Aesar (95%) and purified according to a published procedure.⁴ Deionized water ($\geq 18 \text{ M}\Omega\cdot\text{cm}$) was obtained from a Milli-Q Reference water purification system.

Buffers for barium-133 (^{133}Ba) and radium-223 (^{223}Ra) cation exchange experiments were prepared using ultra-trace elemental analysis grade H_2O (Fisher Chemical), Suprapur NaCl (99.99%, Sigma-Aldrich, St. Louis, MO, USA), and MES hydrate ($\geq 99.5\%$, BioXtra, Sigma-Aldrich) or HEPES ($\geq 99.5\%$, Sigma-Aldrich). Each buffer was adjusted to the desired pH using a small volume of concentrated sodium hydroxide (semiconductor grade, 99.99% trace metals basis, Sigma-Aldrich) in ultra-trace elemental grade H_2O . Buffers for ^{223}Ra solvent extraction experiments were prepared using deionized H_2O , NaNO_3 (extra pure, Acros Organics), and lactic acid (1 N, LabChem). Each buffer was adjusted to the desired pH using a small volume of concentrated sodium hydroxide (semiconductor grade, 99.99% trace metals basis, Sigma-Aldrich) in deionized H_2O .

1.2 Radioisotope Quality Control and Counting

1.2.1 General

^{223}Ra was purchased from the National Isotope Development Center (NIDC) as a dried-down nitrate salt with a specific activity of 5.123×10^4 Ci/g (carrier free), a radionuclidic purity of 99.99%, and a chemical purity of 99%. Upon receipt, it was reconstituted in 10 mM HCl (Fisher Optima HCl and Fisher ultra-trace elemental analysis grade H_2O) to yield a stock solution of approximately 74 kBq $^{223}\text{Ra}/\mu\text{L}$ ($2 \mu\text{Ci } ^{223}\text{Ra}/\mu\text{L}$), unless otherwise noted. From this stock solution, working solutions containing 0.74 kBq $^{223}\text{Ra}/\mu\text{L}$ ($0.02 \mu\text{Ci } ^{223}\text{Ra}/\mu\text{L}$) were prepared prior to each experiment by further dilution with 10 mM HCl.

^{133}Ba was purchased from NIDC as a 2,479 kBq/ μL ($67 \mu\text{Ci}/\mu\text{L}$) stock solution in 0.5 M HNO_3 with a specific activity of 19.76 Ci/g and a radionuclidic purity of >99.9%. Working solutions of 0.74 kBq $^{133}\text{Ba}/\mu\text{L}$ ($0.02 \mu\text{Ci } ^{133}\text{Ba}/\mu\text{L}$) were prepared as needed by further dilution of this stock solution with H_2O .

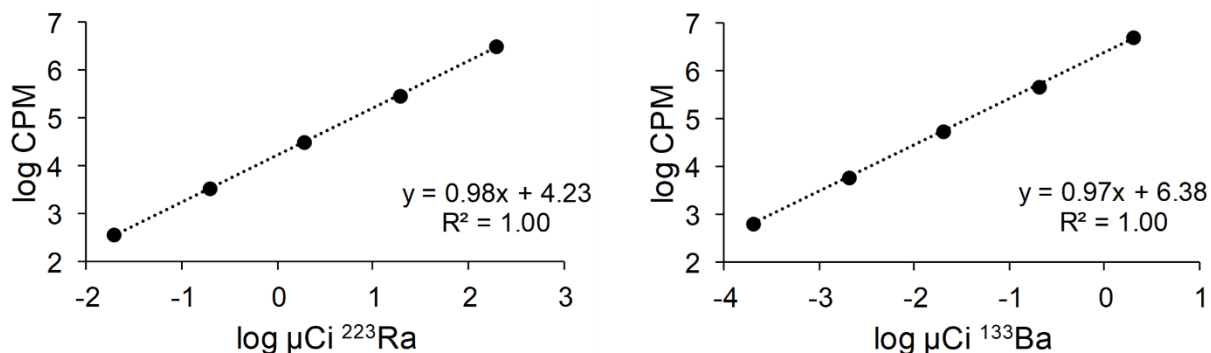
1.2.2 Gamma spectroscopy

The radioisotopic purity and activity of ^{223}Ra and ^{133}Ba were verified by gamma spectroscopy using a Gamma Analyst Integrated Gamma Spectrometer (Canberra), which consists of a high-purity germanium (HPGe) detector (model GC-GA1), U-type cryostat, and automatic sample changer. The detector energy and efficiency were calibrated using a mixed gamma point source containing ^{57}Co , ^{60}Co , ^{88}Y , ^{109}Cd , ^{113}Sn , ^{137}Cs , ^{139}Ce , ^{203}Hg , and ^{241}Am , traceable to the National Institute of Standards and Technology (NIST) and supplied by Eckert & Ziegler Analytics (Atlanta, GA, USA). Samples to be counted were prepared by adding 10 μL of ^{223}Ra or ^{133}Ba working solution into 12 \times 75 mm polypropylene test tubes. Counting dead time was maintained below 5% for all measurements. Data was analyzed using Genie 2000 software (v3.2.1 Canberra). The spectra of these samples can be found in Appendix A (Figures A1 and A2).

1.2.3 Liquid scintillation counting

Samples for liquid scintillation counting (LSC) were prepared by adding 0.1–0.5 mL of aqueous phase or 0.1 mL of organic phase to 5 mL of Ultima Gold liquid scintillation cocktail (PerkinElmer, Waltham, MA, USA) in standard polyethylene scintillation vials (20 mL) equipped with polyethylene cone caps. The samples were mixed by inversion at least three times and counted using a Tri-Carb 4910TR liquid scintillation counter (PerkinElmer). The energy window was set at 0–2,000 keV. ^{223}Ra samples were counted at least 15 h post-preparation to allow sufficient time

for radioactive equilibrium to be reached between ^{223}Ra and its decay chain. ^{133}Ba samples were counted immediately. Counting of each sample was terminated once the 2σ uncertainty in the count rates reached 0.5% or after 1 h, whichever criterion was reached first. Each sample count rate was decay corrected to the time at the start of the LSC analysis. In separate experiments, the count rate was determined to be linear over the range of 0.00074–7.4 kBq (0.020–200 nCi) of ^{223}Ra and 0.0074–74 kBq (0.2–2000 nCi) of ^{133}Ba :



To ensure sample counts were not being attenuated by quenching, tests were conducted in which aliquots of ^{223}Ra radiotracer in 5 mL Ultima Gold cocktail were counted before and after the addition of an aliquot of the highest concentration of macropa, DOTA, or HDEHP used in each solvent system (0.1 mL for solvent extraction system and 0.5 mL for ion exchange system). The counts per minute (CPM) before and after addition of each ligand solution were indistinguishable, indicating that none of the components used in the stability constant studies caused quenching. As such, no quench correction on the collected data was carried out.

Ligand	Concentration (M)	Solvent System	CPM Before Addition	CPM After Addition
DOTA	1.0×10^{-3}	pH 7.68 HEPES/NaCl	298,509	301,250
DOTA	7.1×10^{-4}	pH 8.07 HEPES/NaCl	31,281	31,512
DOTA	5.0×10^{-4}	pH 8.46 HEPES/NaCl	1,823,350	1,824,208
macropa	6.0×10^{-5}	pH 5.62 MES/NaCl	254,382	255,511
macropa	3.9×10^{-5}	pH 5.92 MES/NaCl	254,412	258,484
macropa	8.0×10^{-6}	pH 6.29 MES/NaCl	253,170	254,052
macropa	4.0×10^{-3}	pH 4 lactate/ NaNO_3	522,083	532,288
HDEHP	1.0	<i>o</i> -xylene	518,960	529,882

1.3 Protonation Constants and Non-Radioactive Complex Stabilities by Potentiometric Titration

Protonation constants and alkaline earth (AE) stability constants of macropa and DOTA were obtained by potentiometric titration using either a Metrohm Titrando 888 titrator or an 855 Robotic Titrosampler connected to an 805 Dosimat. Both titration systems were equipped with Ross Orion combination electrodes (8103BN, ThermoFisher Scientific), Metrohm 806 exchange units with automatic burets (10 mL), and *Tiamo 2.5* software. The titration vessel was fitted with a removable glass cell and thermostated at 25 °C using an Isotemp 500LC recirculating chiller (Fisher Scientific). CO₂ was excluded from the titration vessel using a small positive pressure of argon bubbled through 30 wt % KOH. Carbonate-free NaOH (~0.2 M) was prepared using freshly boiled H₂O (≥18 MΩ·cm) and semiconductor-grade NaOH pellets (99.99% trace metals basis, Sigma-Aldrich, stored under Ar). The NaOH solution was standardized against potassium hydrogen phthalate (BioXtra, ≥99.95%, Sigma-Aldrich). HCl (0.1 M, Metrohm Certified Titrants) was titrated against Tris base (Ultrapure Bioreagent, J.T. Baker) to verify its concentration. Potassium hydrogen phthalate and Tris base were both dried in an oven for at least 2 h at 110 °C prior to use. All titration solutions were maintained at a constant ionic strength of 0.2 M using NaCl (BioUltra, ≥99.5%, Sigma-Aldrich) and equilibrated for 25 min prior to the addition of titrant.

Before every ligand or ligand/metal titration, the electrode was calibrated in terms of the hydrogen-ion concentration by titrating a solution of standardized HCl (0.005 M) containing supporting electrolyte (NaCl = 0.195 M) with standardized NaOH. Data within the pH ranges of 2.3–3.2 and 10.8–11.3 were analyzed using the program *Glee* (version 3.0.21)⁵ to obtain the standard electrode potential (E_0) and slope factor. The H₂O ion product ($pK_w = 13.74$) was taken from the literature.^{5,6} Stock solutions of macropa and DOTA were prepared in MQ H₂O and their exact concentrations were determined potentiometrically using a standardized KOH solution (0.1 M). Specifically, the concentration of the macropa stock solution was determined from the two sharp endpoints of its titration curve using the formula $((V_{EP2} - V_{EP1})/npK_a) * [KOH]$. The concentration of the DOTA stock solution was determined by potentiometric titration in the absence and presence of a ~40-fold excess of Ca²⁺ (CaCl₂ hydrate, 99.999%, Beantown Chemical) using the formula $((V_{EP,+Ca} - V_{EP,-Ca})/npK_a) * [KOH]$. ICP standards of calcium, strontium, and barium in dilute HNO₃ were employed in the metal-ligand titrations. The exact amount of HNO₃ in each standard was determined from the endpoint of triplicate titrations with standardized KOH.

The protonation constants of macropa and DOTA and stability constants of their cold AE^{2+} complexes were measured by adding standardized NaOH to an aqueous solution (20 mL) of ligand (0.02 mmol), mineral acid (0.1 mmol HCl for ligand titrations and 0.1 mmol HCl/NO₃ for metal-ligand titrations), and NaCl (3.9 mmol) in the absence and presence of an equimolar amount of AE^{2+} metal ion (0.02 mmol), respectively. The titration method employed a 0.1 mV min⁻¹ drift limit and a maximum wait time of 180 s (ligand titrations) or 300 s (metal-ligand titrations) between additions of aliquots of base. For metal-ligand titrations, further implementing a minimum wait time of either 0 s or 60 s between additions of base gave rise to the same stability constant values upon data refinement, indicating that equilibrium was attained rapidly after each addition of base in all AE/ligand systems.

The protonation and stability constants were refined using the program *Hyperquad2013*.⁷ Only the proton concentration was admitted as a refinable parameter. The protonation constants, defined in Eq. S1 below and compiled in Table S1, were calculated from the average of at least three independent titrations, with >60 data points for each titration. The protonation constants measured for macropa in 0.2 M NaCl are similar to those reported in 0.1 M KCl.^{3,8} The slight increase in the value of log K_{a1} (7.94) in 0.2 M NaCl in comparison to the value of log K_{a1} (7.41) obtained in 0.1 M KCl suggests that macropa binds more strongly to the K⁺ ion than it does to the Na⁺ ion. This observation is consistent with macropa's higher affinity for larger over smaller metal ions. The protonation constants measured for DOTA in 0.2 M NaCl are generally consistent with those previously reported in 0.1 M NaCl⁹ and 0.15 M NaCl,¹⁰ which are shown in Table S1 for comparison. Specifically, we find log K_{a2-5} to be 9.54, 4.44, 3.99, and 2.14 in 0.2 M NaCl, whereas values of 9.21, 4.48, 4.03, and 1.99 are reported in 0.15 M NaCl¹⁰ and values of 9.14, 4.63, and 3.91 are reported in 0.1 M NaCl (no log K_{a5} value was reported in this reference).⁹

Furthermore, our results indicate that the first protonation constant of DOTA (log K_{a1} = 8.79) is lower than its second protonation constant (log K_{a2} = 9.54) in 0.2 M NaCl medium. A similar, albeit less pronounced, trend was also observed in 0.15 M NaCl (log K_{a1} = 9.14, log K_{a2} = 9.21).¹⁰ This apparent reversal in protonation constants arises from strong complex formation between Na⁺ and DOTA (log K_{ML} = 4.2 at 25 °C and 0.1 M N(CH₃)₄NO₃/Cl),¹¹ which leads to a reduction in log K_{a1} relative to log K_{a2} as the concentration of Na⁺ increases. The validity of our findings that log K_{a1} < log K_{a2} for DOTA is supported by examining literature values for the protonation constants of DOTA in various media. Specifically, the value of log K_{a1} for DOTA decreases from

~**11.9–12.60** in 0.1 M Me₄NCl^{11,12} to **11.14** in 0.1 M KCl⁹ to **9.37** in 0.1 M NaCl, reflecting an increase in complex formation between DOTA and the background electrolyte cation upon moving from NMe₄⁺ to K⁺ to Na⁺ media. Log K_{a1} is reported to decrease further to **9.14** when the concentration of NaCl is increased to 0.15 M.¹⁰ We note that in this reference, they also reported a value for log K_{a1} (9.14) that is lower than that of log K_{a2} (9.21). Collectively, these data suggest that upon moving to an even higher concentration of NaCl, the value of log K_{a1} will be reduced further. This trend is borne out in our titrations in 0.2 M NaCl, which provide a log K_{a1} of **8.79**.

With the protonation constants in hand, the stepwise stability constants (Eq. S2 below) and protonation constants of the metal complexes (Eq. S3 below) were calculated from the average of at least three titrations, with >60 data points for each titration. Hydrolysis constants for the formation of [AE(OH)]⁺ in aqueous solution were included in the model.¹³ The errors provided correspond to 1 standard deviation. Although protonated AE complexes have been reported previously for DOTA in 0.1 NMe₄Cl/NO₃ media,^{11,12} these species could not be reasonably modeled from our data in 0.2 M NaCl. The log K_{ML} values of 11.45, 9.70, and 6.06 obtained for macropa with Ba²⁺, Sr²⁺, and Ca²⁺, respectively, in 0.2 M NaCl are similar to the literature values of 11.11 (0.1 M KCl), 9.57 (0.1 M KNO₃), and 5.25 (0.1 M KNO₃) obtained in different background electrolytes.^{8,14} Specifically, our stability constants are only slightly higher than those reported in K⁺ medium, which probably arises from slight differences in the affinity of macropa for Na⁺ versus K⁺ (see above).

$$K_{ai} = \frac{[H_iL]}{[H_{i-1}L][H^+]} \quad (S1)$$

$$K_{ML} = \frac{[ML]}{[M][L]} \quad (S2)$$

$$K_{MH_nL} = \frac{[MH_nL]}{[MH_{n-1}L][H]} \quad (S3)$$

1.4 ²²³Ra Stability Constant Determination: Solvent Extraction Method

1.4.1 Organic phase preparation

HDEHP solutions were prepared at the desired concentration (0.2 M or 1 M) in *o*-xylene by diluting weighed portions of HDEHP up to known volumes in volumetric flasks. Each organic phase was pre-conditioned with the appropriate buffer (pH 3 lactate/NaNO₃ or pH 4 lactate/NaNO₃, see below) by mixing equal volumes of organic and aqueous phases at room temperature. The phases were separated by centrifugation and the organic phase was recovered. Fresh buffer was

added, and the procedure was repeated 2–6 times until the pH of the contacted aqueous phase matched that of fresh, uncontacted buffer.

1.4.2 Aqueous phase preparation

An aqueous stock solution of macropa was prepared in H₂O and its exact concentration was determined by potentiometric titration with KOH (see Section 1.3). It was subsequently used to prepare buffered solutions of macropa (4.07 mM) at pH 3 and pH 4 in 0.05 M lactate/1 M NaNO₃. Lactate buffer (0.05 M) containing 1 M NaNO₃ in the absence of ligand was also prepared at pH 3 and pH 4 in a similar manner. The electrode used to measure the pH of the solutions was filled with 3 M NaCl and calibrated daily by potentiometric titration of 0.005 M HNO₃/0.995 M NaNO₃ between pH 2.3 and 11.3 with 0.1 M NaOH/0.9 M NaNO₃. From separate titrations of HNO₃ in NaNO₃ media, the ionic product of water, or pK_w , of 13.69 was experimentally determined at $I = 1$ M and $T = 25$ °C.

1.4.3 Liquid-liquid extraction

Solvent extraction experiments were conducted at 25 °C in 2 mL screw-capped polypropylene tubes fitted with o-rings. The buffered aqueous phase containing macropa (0.585 mL, 4.07 mM macropa) was spiked with ²²³Ra (0.015 mL, 4.995 kBq or 135 nCi in 10 mM HNO₃) and contacted with the HDEHP/*o*-xylene organic phase (0.6 mL, 0.2 M or 1 M HDEHP) for 1 h by end-over-end rotation at 40 RPM. Control samples were also prepared in which macropa was omitted from the aqueous phase. The samples were centrifuged at 8600 RPM for 3 min, and an aliquot of each phase (0.1 mL) was carefully removed and analyzed by LSC (see Section 1.2.3). Distribution coefficients (D_{Ra}) were calculated as the ratio of the activity detected in the organic phase versus the activity in the aqueous phase after extraction (CPM_{org}/CPM_{aq}), with activity being proportional to the concentration of ²²³Ra in each phase.

1.4.4 Results

The results of the solvent extraction study are summarized in Figure S1. Unexpectedly, at both pH 3 and pH 4 using HDEHP concentrations of 0.2 M and 1 M, we observed higher D_{Ra} values for samples in which macropa was included in the aqueous phase relative to samples in which the complexant was omitted (D_0). This increase in partitioning of ²²³Ra to the organic phase rather than to the aqueous phase is opposite of what is anticipated based on macropa's ability to chelate Ra²⁺ in aqueous solution.¹⁵ This trend was also unexpected based on literature precedent, which demonstrates that stability constants of complexes of macropa with other radioactive metal ions,

namely $^{244}\text{Cm}^{3+}$ and $^{241}\text{Am}^{3+}$, can be determined successfully using this biphasic solvent extraction system.^{16,17} Although we note that in these preliminary experiments, the extraction kinetics of the samples were not measured, we do not anticipate that a lack of complete equilibration would give rise to consistently higher D_{Ra} values for samples in which macropa is present in the aqueous phase versus when it is absent. Rather, we hypothesize that the observed trend arises from solubilization of the $[\text{}^{223}\text{Ra}(\text{macropa})]$ complex in the organic phase. The origin of this solubility may arise from the neutral charge of the complex in conjunction with the high concentrations of HDEHP required to load the organic phase with $^{223}\text{Ra}^{2+}$. These high concentrations of HDEHP may increase the polarity of the *o*-xylene organic phase, leading to enhanced solubilization of macropa complexes. By contrast, macropa predominately forms +1 or +2 complexes with Cm^{3+} and Am^{3+} under similar conditions.¹⁶ These charged complexes are expected to be less soluble in an HDEHP/*o*-xylene organic phase than a neutral complex. Furthermore, only low concentrations of HDEHP (< 0.02 M) were required to load the organic phase with Cm^{3+} and Am^{3+} in these experiments, owing to the higher affinity of HDEHP for more charge dense +3 ions. Although additional studies are needed to confirm our hypothesis that $[\text{}^{223}\text{Ra}(\text{macropa})]$ is soluble in HDEHP/*o*-xylene under our experimental conditions, our preliminary results suggest that this solvent extraction system is not suitable to determine the stability constant of the $[\text{}^{223}\text{Ra}(\text{macropa})]$ complex. As such, an alternative method of cation exchange was explored to determine Ra^{2+} stability constants.

1.5 ^{133}Ba and ^{223}Ra Stability Constant Determination: Cation Exchange Method

1.5.1 Resin conditioning

Dowex 50W X8 resin (hydrogen form, 200–400 mesh, 60 g, Sigma-Aldrich) was contacted with 2 M HCl (~50 mL, prepared using Optima HCl and MQ H₂O) by end-over-end rotation for 2 h to remove any metal impurities. The suspension was passed through a polypropylene column equipped with a 20 μm polyethylene frit, and then the filtered resin was soaked for another hour in fresh 2 M HCl. After removing the HCl from the column using a positive pressure of air, the resin was washed with MQ H₂O (2 \times 40 mL) to remove excess acid, and then converted to the Na^+ form using 1 M NaOH (3 \times 40 mL). The NaOH solution was prepared from semiconductor grade pellets (99.99% trace metals basis, Sigma-Aldrich) and MQ H₂O. The pH of the final NaOH washing was ~12 by litmus paper, signaling complete conversion of the resin from the H^+ form to the Na^+ form. Lastly, the resin was washed free of adhering NaOH solution using H₂O (7 \times 40 mL), until the pH of the filtrate was reduced to 7 by litmus paper. The resin was spread out to air-

dry on glassine paper for three days and then stored in an acid-washed media bottle. The mass of the dried resin was 37 g.

1.5.2 Sample preparation and workup

A series of MES (pH 5.62, 5.92, 6.29) and HEPES (pH 6.67, 7.19, 7.45, 7.68, 8.07, 8.46) buffers were prepared at a concentration of 0.025 M and a total ionic strength of 0.2 M (buffer + NaCl) as described in Section 1.1. The pH of each buffer was determined at 25 °C using a glass electrode calibrated by titration of 0.005 M HCl/0.195 M NaCl from pH 2.3 to 11.3 with 0.2 M NaOH. Stock solutions of macropa and DOTA were prepared in ultra-trace water (Fisher) and their concentrations were determined by potentiometric titration using the methods described in Section 1.3. From these stock solutions, buffered sub-stock solutions of the ligands were prepared in MES (macropa) or HEPES (DOTA) by dilution to a desired final concentration in a volumetric flask. The pH of these sub-stock solutions was carefully re-adjusted with NaOH to match the pH of the respective parent buffers. This pH adjustment was necessary because of the relatively large contribution of acid from the ligands, which exceeded the buffering capacity of MES/HEPES at the concentrations used. Each buffered sub-stock solution was then used to prepare a series of solutions of varying ligand concentration by further dilutions with the appropriate buffer. This procedure ensured that the pH of every sample across a concentration series was both constant and precisely matched to the parent buffer solutions.

Samples for distribution experiments were subsequently prepared by adding aliquots (1 mL) of ligand solution to screw-capped polypropylene tubes containing 25 ± 0.5 mg of Dowex resin. The samples were spiked with 10 μ L (200 nCi, 7.4 kBq) of ^{223}Ra or ^{133}Ba working solution (Section 1.2.1) and mixed by end-over-end rotation at 40 RPM and 25 °C. After equilibrium was reached (see note below), samples were centrifuged at 8600 RPM for 3 min, and an aliquot (0.5 mL) of supernatant was removed for LSC (Section 1.2.3). The equilibrium pH of select samples was also measured and matched that of the parent buffer, indicating that the sample pH did not change upon contact with the resin. The experiments were performed in triplicate for ^{223}Ra with DOTA (pH 7.68, 8.07, 8.46) and macropa (pH 5.62, 5.92, 6.29), with each pH/concentration series containing at least 10 data points. Likewise, ^{133}Ba experiments were performed for macropa (pH 5.62 MES, n = 3; pH 5.91 MES, n = 1) and DOTA (pH 6.67 HEPES, n = 3; pH 7.19 HEPES, n = 5; and pH 7.45 HEPES, n = 3), and served to verify that pH-independent stability constants, or log

K_{ML} values, obtained via the radiotracer technique closely match those obtained using macroscopic amounts of metal ion.

Control samples were also prepared in which buffer only (no ligand) was added to tubes in the absence or presence of resin. The control samples without resin provide the total activity of ^{223}Ra or ^{133}Ba , A_{tot} , in each sample, expressed in CPM. This value is proportional to the concentration of radionuclide in each sample, less any radiometal adsorbed onto the walls of the tubes. No tube-to-tube variation was observed in A_{tot} , indicating that any adsorption on the tube walls is reproducible irrespective of the tube used. The control samples with resin provide the distribution ratio of the radioisotope in the absence of ligand, D_0 . D_0 was found to be constant irrespective of sample pH, which is consistent with the chemical structure of Dowex 50. Specifically, this resin contains highly acidic sulfonic acid functional groups as the sole ion-active group. These groups are deprotonated across the common pH working range of 0–14, rendering the ion-exchange efficiency of the resin unaffected by changes in $[\text{H}^+]$.¹⁸ Finally, control experiments were also performed with ^{223}Ra in which MES and HEPES buffers were replaced with 0.2 M NaCl only. No change in D_0 was noted for these samples in comparison to samples in which buffering agents were included, signaling that MES and HEPES do not effectively bind the Ra^{2+} ion. As such, Ra-MES and Ra-HEPES complexes were not considered in the complexation model when refining the data.

Note on sample equilibration: Preliminary studies indicated that equilibrium was reached in under 24 h for all ligand/pH systems. However, because DOTA is well known for exhibiting slow binding kinetics with most metal ions, we took extra precautions to ensure all samples were at equilibrium before workup. Specifically, replicates were spiked with radiotracer at the same time but centrifuged and sampled on different days for most series. This varying mixing time for replicates allows for the detection of very slow equilibration over days, which would manifest as differences in distribution ratios among replicates. No such differences were observed between replicates; the stability constants calculated from these data were identical, signaling that equilibrium was reached in all our samples.

1.5.3 Effects of metal contaminants

Initial stability constant measurements of $[\text{Ra}(\text{macropa})]$ using the cation exchange technique were performed at pH 12.4 and an ionic strength of 0.2 M, matching the conditions recently reported to be effective for determining the stability constant of the $[\text{Ra}(\text{EDTA})]^{2-}$ complex.¹⁹

From these experiments, however, we did not obtain the expected linear trend upon plotting $D_0/D-1$ versus free ligand concentration (see Section 1.5.4, Data Analysis). Instead, our plots revealed two distinct regions of differing slopes, as shown in Figure S9. At low ligand concentration, the data is best fit by a linear model with a near-zero intercept but a small slope, whereas at high ligand concentration, the data is best fit by a linear model with a negative y-intercept and a larger slope. We attribute this deviation from linearity to the presence of trace metal contaminants in the samples, which compete with the ultra-trace amount of $^{223}\text{Ra}^{2+}$ ions in solution for binding to macropa $^{2-}$. Similar results were also observed when the experiment was repeated using EDTA. We hypothesize that these competing metals consume a substantial fraction of the total amount of macropa present in solution when the ligand concentration is relatively low, thereby reducing the amount of macropa $^{2-}$ available to bind Ra^{2+} relative to the theoretical value calculated based on total ligand concentration and $\text{p}K_a$ values. This problem was probably not observed in previous stability constant studies for radium complexes because these efforts used the longer-lived isotopes ^{226}Ra and ^{228}Ra ,^{19–24} which afford higher concentrations of the Ra^{2+} ion in solution at activities similar to those used here with ^{223}Ra . Furthermore, many of these earlier studies required the use of millimolar concentrations of ligand to partition Ra^{2+} to the aqueous phase, reflecting the lower affinity of these ligands for Ra^{2+} . Under these conditions of excess ligand, small amounts of metal contaminants can be scavenged without significantly impacting the free ligand concentration. By contrast, only low concentrations of macropa, on the order of 10^{-7} – 10^{-8} M, are needed to partition Ra^{2+} to the aqueous phase at pH 12.4, which reflects the high binding strength of macropa for this metal ion. In this low concentration regime, the impact of metal impurities is significant.

These findings prompted us to take extreme measures to exclude potential introduction of trace metal impurities into our experiments. These efforts included passing our pH 12.4 solutions through Chelex before use, purchasing the highest purity NaOH and NaCl available, and acid washing all plasticware and glassware before use. Despite these precautions, we did not see any improvement in the quality of fit of our data under these conditions. As such, these extreme measures were discontinued. We instead adopted a different approach in which the pH of the samples was reduced (e.g., to pH 5.6–8.5). Under these lower pH conditions, the *concentration of fully deprotonated macropa* (free chelator) present in the samples is the same as the concentrations of macropa used at pH 12.4 (10^{-7} – 10^{-8} M), but the *total concentration of macropa* that can be used in each sample is orders of magnitude higher ($\sim 10^{-5}$ M) because the effective binding strength of

macropa is reduced at lower pH values. This increase in total macropa concentration used in each sample brought us into a regime in which enough macropa is present to scavenge the trace metal impurities without significantly impacting the amount of free, fully deprotonated macropa present in solution. Using this approach, we were successfully able to obtain the expected linear fit of $(D_0/D)-1$ as a function $[\text{macropa}^{2-}]$. A similar approach was used for cation exchange experiments with DOTA.

1.5.4 Data analysis

Fully deprotonated ligand concentration ($L^{n-} = [\text{macropa}^{2-}]$ or $[\text{DOTA}^{4-}]$) in each sample was calculated from total ligand concentration, solution $p[H]$, and ligand protonation constants determined in 0.2 M NaCl (Table S1 and Fig. S2–S6), using the normal assumption that the metal ion concentration does not affect the concentration of the free ligand. This assumption is valid because total ligand concentration was, in all cases, at least several orders of magnitude higher than the radiotracer concentration. Distribution coefficients (D values) were taken as the ratio of activity in the resin versus activity in the aqueous phase ($\text{CPM}_{\text{resin}}/\text{CPM}_{\text{aq}}$) at equilibrium, where $\text{CPM}_{\text{resin}} = \text{CPM}_{\text{total}} - \text{CPM}_{\text{aq}}$. From these distribution ratios of ^{223}Ra or ^{133}Ba in the absence (D_0) or presence (D) of varying concentrations of ligand, a conditional cumulative stability constant, β_{app} , of metal–ligand complexation can be determined according to equations S4–12 below. Metal (M) and complex charges are omitted for clarity.

$$[M]_{\text{initial}} = [M]_{\text{resin}} + [M]_{\text{total, aq}} \quad (\text{S4})$$

$$[M]_{\text{total, aq}} = [M]_{\text{free}} + [M]_{\text{complexed}} \quad (\text{S5})$$

$$\beta_{\text{app}} = \frac{[M]_{\text{complexed}}}{[M]_{\text{free}} [L^{n-}]} \quad (\text{S6})$$

Rearrangement and substitution of equation S5 into equation S6 provides equation S7:

$$\beta_{\text{app}} = \frac{[M]_{\text{total, aq}} - [M]_{\text{free}}}{[M]_{\text{free}} [L^{n-}]} \quad (\text{S7})$$

Rearrangement of S7 and further reduction yields S8:

$$\beta_{\text{app}} [L^{n-}] = \frac{[M]_{\text{total, aq}} - [M]_{\text{free}}}{[M]_{\text{free}}} = \frac{[M]_{\text{total, aq}}}{[M]_{\text{free}}} - \frac{[M]_{\text{free}}}{[M]_{\text{free}}} = \frac{[M]_{\text{total, aq}}}{[M]_{\text{free}}} - 1 \quad (\text{S8})$$

Upon further rearrangement of equation S8, equation S9 is obtained:

$$[M]_{\text{total, aq}} = (\beta_{\text{app}} [L^{n-}] + 1) * [M]_{\text{free}} \quad (\text{S9})$$

$$\text{Without ligand} \rightarrow D_0 = \frac{[M]_{resin}}{[M]_{free}} = \frac{[M]_{initial} - [M]_{total, aq}}{[M]_{free}} \quad (\text{S10})$$

$$\text{With ligand} \rightarrow D = \frac{[M]_{resin}}{[M]_{total, aq}} = \frac{[M]_{initial} - [M]_{total, aq}}{[M]_{free}(\beta_{app}[L^{n-}] + 1)} = \frac{D_0}{\beta_{app}[L^{n-}] + 1} \quad (\text{S11})$$

Rearrangement of S11 provides S12:

$$\frac{D_0}{D} - 1 = \beta_{app}[L^{n-}] \quad (\text{S12})$$

As indicated above, β_{app} is a conditional cumulative stability constant for metal–ligand complexation that is only valid for the pH at which it is determined. This overall constant is further defined in equation S13, assuming the formation of only 1:1 M:L complexes.

$$\beta_{app} = \sum \beta_{mhl} [H^+]^h [L] \quad (\text{S13}),$$

wherein β_{mhl} is the stability constant for the complex MH_hL .²⁵ A metal–ligand stoichiometry of 1:1 for complexation of ¹³³Ba or ²²³Ra by DOTA and macropa was confirmed from the slopes obtained through linear regression analyses of $\log(D_0/D - 1)$ versus $\log[\text{macropa}^{2-}]$ or $\log[\text{DOTA}^{4-}]$ (Fig. S7, S8 and Tables S2 and S3).

To further derive the pH-independent stability constant, or $\log K_{ML}$ value, and the stepwise stability constants of any protonated metal–ligand complexes, experiments were run at several different pH values (macropa, p[H] 5.62–6.29; DOTA, p[H] 7.68–8.46, Figs. S9–15).^{16,26} These experiments revealed that the values of β_{app} for complexation of ²²³Ra by both macropa and DOTA remained constant with varying sample acidity, supporting the absence of protonated complexes in solution over the pH range investigated (see Figures S16 and S17). Therefore, β_{app} could be taken as the K_{RaL} value. The $\log \beta_{app}$ ($\log K_{RaL}$) values from triplicate measurements at each pH were averaged (Table S4). These values were subsequently averaged across pH to provide the $\log K_{RaL}$ values shown in the main text Table 1 for $[\text{Ra}(\text{macropa})]^{2-}$ and $[\text{Ra}(\text{DOTA})]^{4-}$.

1.5.5 Correction of $[\text{Ra}(\text{DOTA})]^{2-}$ stability constant for Na^+ binding

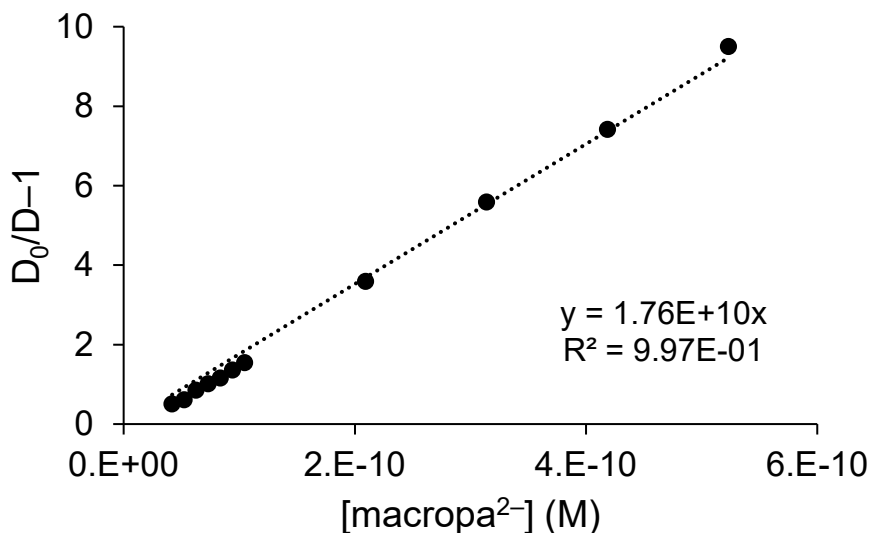
As described in Section 1.5.4, the fully deprotonated ligand concentrations, $[L^{n-}]$, for macropa and DOTA used in equation S12 were calculated from total ligand concentration, solution p[H], and ligand protonation constants determined in 0.2 M NaCl. However, DOTA is known to form a

strong complex with Na^+ , which will decrease the free concentration of $[\text{DOTA}^{4-}]$ available to bind the Ra^{2+} ion. To account for this interaction, the titration data for DOTA in 0.2 M NaCl were simultaneously refitted by inclusion of the $[\text{Na}(\text{DOTA})]^{3-}$ stability constant ($\log K = 4.2$)¹¹ into the model in *Hyperquad*. In this way, Na-independent $\text{p}K_a$ values were obtained for DOTA ($K_{a1} = 12.29$, $K_{a2} = 9.54$, $K_{a3} = 4.43$, $K_{a4} = 4.00$, $K_{a5} = 2.14$). These values closely match those published previously for DOTA in 0.1 M $\text{NMe}_4\text{Cl}/\text{NO}_3$.¹¹ With these Na-independent protonation constants in hand, the free DOTA concentration for each sample was subsequently re-calculated according to equation S14 and used in equation S12 to obtain a Na-independent $\log K_{\text{ML}}$ value for the $[\text{Ra}(\text{DOTA})]^{2-}$ complex.

$$[\text{DOTA}^{4-}]_{\text{free}} = [\text{DOTA}^{4-}]_{\text{total}} * \frac{\beta_4}{[\text{H}^+]^4 + \beta_1[\text{H}^+]^3 + \beta_2[\text{H}^+]^2 + \beta_3[\text{H}^+] + \beta_4 + \beta_4 K_{\text{NaDOTA}}[\text{Na}^+]} \quad (\text{S14})$$

1.5.6 ¹³³Ba distribution measurements at low pH

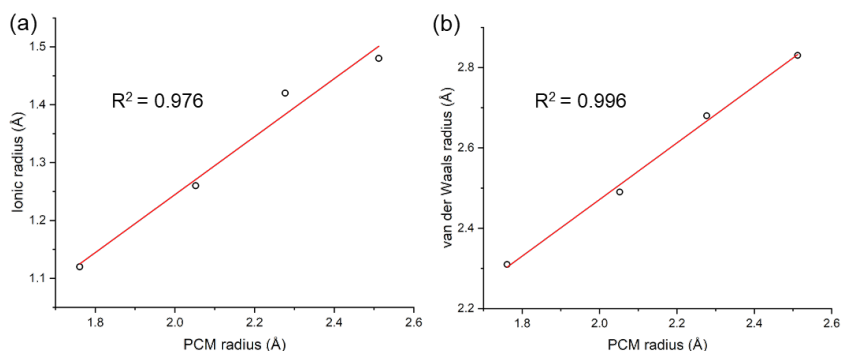
To probe the utility of the cation exchange method for detection of protonated complexes of Ba^{2+} with macropa (e.g., MHL and MH_2L), which are reported to exist via potentiometric titration using nonradioactive Ba^{2+} , a distribution experiment was performed at $\text{p}[\text{H}]$ 3.92 (25 mM sodium formate, $I_{\text{tot}} = 0.2$ M with NaCl). This $\text{p}[\text{H}]$ was selected such that the total macropa concentration required to obtain measurable distributions was below 5 mM. Conducting experiments at lower pH values necessitates the use of higher concentrations of macropa to obtain accurate distribution ratios, such that an ionic strength of 0.2 M cannot be maintained, and the overall composition of the solutions cannot be considered similar to measurements conducted at higher $\text{p}[\text{H}]$ values (lower macropa concentrations). The value for $\log \beta_{\text{app}}$ at $\text{p}[\text{H}]$ 3.92 was found to be only 10.25 (see graph below). This value is nearly 1 order of magnitude lower than value for $\log \beta_{\text{app}}$ measured at higher $\text{p}[\text{H}]$ (Figures S18 and S19). This trend is the opposite of that expected when protonated complexes are formed at low $\text{p}[\text{H}]$. Specifically, the $\log \beta_{\text{app}}$ value should increase with decreasing pH. We attribute this underestimated β_{app} value to the adsorption of cationic ligand (e.g., $\text{H}_3\text{macropa}^+$) and/or complex (e.g. $[\text{Ba}(\text{Hmacropa})]^+$) species onto the cation exchange resin. Ultimately, these results show that this Dowex method is not suitable for determining the stability constants of protonated Ba–macropa complexes. The exploration of other resins that are compatible with positively charged species will be the focus of future research efforts.



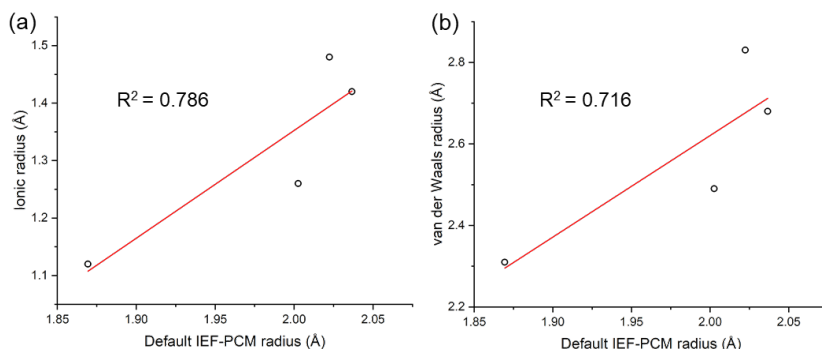
1.6 Density Functional Theory Calculations

Electronic structure calculations were performed using the Gaussian 16, rev A.03 software package.²⁷ We used the density functional theory (DFT) approach employing the hybrid B3LYP functional.^{28,29} Standard 6-31+G* and def2TZVPP basis sets were used for main group elements and hydrogen for geometry optimization. The metal atoms were modeled using relativistic small-core (SC) energy-consistent pseudopotentials for the alkaline-earth elements (Ca, ECP10MDF; Sr, ECP28MDF; Ba, ECP46MDF; Ra, ECP78MDF) and the associated basis sets.³⁰ Some diffuse G, F, D, and P functions were purposely offset from the basis set of the metals when used in conjunction with the 6-31+G* basis set for light elements to provide the consistent basis set size for the optimized macrocycle complexes (sample input files of the Gaussian 16 calculations are provided in Appendix B below). Efforts were undertaken to perform a systematic search for various starting geometries of the complexes with the aim of finding the lowest-energy clusters. Therefore, the most stable configuration for each complex was selected for the $\Delta\Delta G^{\text{calc}}_{\text{aq}}$ (Ca²⁺/Ra²⁺; Ba²⁺; Sr²⁺) Gibbs free energy calculations. Frequency calculations at the B3LYP/SC/6-31+G* level were performed to ensure real vibrational modes for the minimum ground state structures and to provide zero point energies (ZPE). Thermal contributions (T = 298.15 K) to the gas phase Gibbs free energies were calculated using standard molecular thermodynamic approximations,³¹ except that vibrational frequencies lower than 60 cm⁻¹ were raised to 60 cm⁻¹. This procedure is based on the so-called quasiharmonic approximation, which was first introduced by Truhlar et al.³² and serves as a way to correct for the well-known breakdown of the harmonic

oscillator model for the free energies of low-frequency vibrational modes. Free energies of solvation were calculated at the B3LYP/SC/6-31+G* level using the IEF-polarizable continuum model (PCM) with the default settings, except for the PCM metal radii, which were set to 1.761 Å (Ca), 2.052 Å (Sr), 2.277 Å (Ba), and 2.512 Å (Ra) according to ref³³ without scaling factors ($\alpha = 1.0$). This step is justified because the chosen PCM radii provide linear relationships with both Shannon's ionic radii³⁴ (a) and van der Waals radii³⁵ (b) of the alkaline-earth elements, supporting the reliability of the selected PCM radii for calculating solvation effects:



By contrast, the default IEF-PCM radii settings fail to show good correlations with the corresponding ionic (a) and van der Waals radii (b), and thus are unlikely to provide reliable hydration energies, as was demonstrated in previous theoretical studies of lanthanide and actinide macrocycle complexes.^{36,37}



It is worth noting that the crystal structures of macropa with Ba^{2+} and DOTA with Sr^{2+} available from the Cambridge Structural Database (CSD) show the presence of one solvent molecule (DMSO/DMF [CCDC 2035004 /CCDC 1883239] or water [CCDC 194130]) in the first coordination sphere of the metal ions. However, it is unclear whether the same coordination environment is retained for the macrocyclic complexes in dilute aqueous solution. Specifically,

the structures of crystalline solids are typically defined by crystal packing forces and long-range electrostatics without accounting for the effects of bulk water on the structure, which could be significant especially in the case of diffuse metal cations like Ra^{2+} . Additionally, our DFT calculations of the $[\text{Ra}(\text{macropa})(\text{H}_2\text{O})]$ and $[\text{Ba}(\text{macropa})(\text{H}_2\text{O})]$ complexes indicate that during geometry optimizations, the inner-sphere water molecule tends to move to the outer sphere to preferentially form a hydrogen bond with the oxygen donor atom of the ligand. Therefore, to avoid the ambiguity related to the potentially different number of water molecules directly coordinating to the metal ion across the alkaline earth series, we have adopted the continuum approach, where the interactions between the solute (metal-ligand complex) and solvent (water) are approximated by creating the molecular cavities of solutes within a dielectric continuum.

Ligand strain energies relative to Ca^{2+} complexation were calculated at the B3LYP/SC/def2TZVPP level of theory as the difference of the ligand's total energies in the corresponding metal bound configurations. Due to electrostatic repulsion of negatively charged donor groups, the equilibrium distance between donor atoms in a free, fully deprotonated ligand is typically larger than the optimal distance for chelating with the largest alkaline earth metal ion, Ra^{2+} . Thus, relative ligand strain would strongly depend on the electrostatic contribution (i.e., the separation distances between negative charges) and almost always decreases with increasing the size of AE^{2+} ion, since $[\text{Ra}(\text{DOTA})]^{2-}$ and $[\text{Ra}(\text{macropa})]$ exhibit the largest separation distance between the negatively charged carboxylate and picolinate groups, respectively. To avoid this bias due to intraligand electrostatics, calculations of relative strain energies reported in Table S8 were performed for the neutral cyclen and diaza-18-crown-6 (D18C6) fragments of DOTA and macropa, where the respective amine nitrogens were terminated with hydrogen atoms.

Chemical bonding analysis was performed for the DFT-optimized structures using the natural bond orbital (NBO) methodology.³⁸ NBO analysis provides a good quantitative description of interatomic and intermolecular interactions in accordance with the basic Pauling–Slater–Coulson representations of bond polarization and hybridization.^{39,40} If the studied complexes are described as Lewis acid (AE^{2+}) bonded to Lewis base (ligand), then the strength of donor (occupied electron lone pairs of the ligand functional groups)–acceptor (vacant valence orbitals of AE^{2+} , n^*_{AE}) interactions would be defined by the Lewis basicity/acidity of the components. The donor–acceptor interaction energy (second-order stabilization energies, $E^{(2)}$) in the NBOs was estimated via second-order perturbation theory (SOPT) analysis of the Fock matrix.³⁹ For each donor orbital

(i) and acceptor orbital (j), the stabilization energy $E^{(2)}$ associated with $i \rightarrow j$ delocalization is given by:

$$E_{ij}^{(2)} = -o_i \frac{\langle i | \hat{F}_{(i,j)} | j \rangle^2}{\epsilon_j - \epsilon_i},$$

where o_i is the donor orbital occupancy, $\hat{F}_{(i,j)}$ is the Fock operator, and ϵ_i and ϵ_j are the orbital energies.

2. SUPPORTING FIGURES, SCHEMES, AND TABLES

2.1 Stability Constant Determination

2.1.1 Solvent extraction method (^{223}Ra)

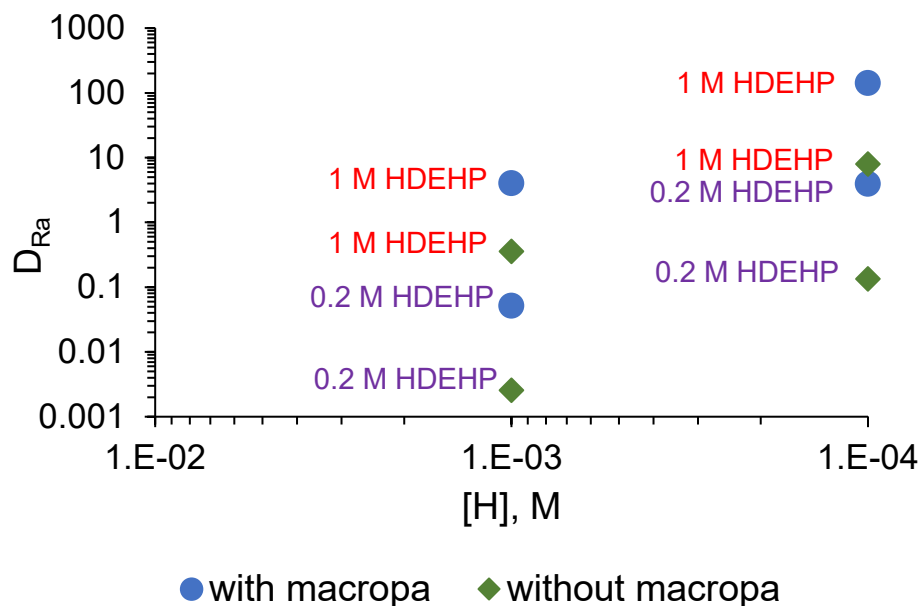


Figure S1. Distribution of ^{223}Ra into HDEHP/*o*-xylene from a buffered aqueous phase in the presence or absence of macropa as a function of pH. Experiments were conducted at pH 3 and pH 4 using 0.2 M or 1 M of HDEHP. Under these conditions, an increase in the distribution of ^{223}Ra to the organic phase was consistently observed when macropa was included in the aqueous phase versus when it was absent.

2.1.2 Potentiometric titration (nonradioactive alkaline earths)

Table S1. Protonation constants of macropa and DOTA determined at 25 °C and I = 0.2 M NaCl.^{a,b}

	macropa ²⁻	DOTA ⁴⁻
log K_{a1}	7.94(2), 7.41, ^c 7.41 ^d	8.79(3), 9.37 ^e , 9.14 ^f
log K_{a2}	6.78(2), 6.85, ^c 6.90 ^d	9.54(2), 9.14 ^e , 9.21 ^f
log K_{a3}	3.29(4), 3.32, ^c 3.23 ^d	4.44(1), 4.63 ^e , 4.48 ^f
log K_{a4}	2.59(5), 2.36, ^c 2.45 ^d	3.99(2), 3.91 ^e , 4.03 ^f
log K_{a5}	1.69 ^c	2.14(2), 1.99 ^f
$\sum \log K_a$	20.6	28.9

^aThe standard deviation is given in parentheses and corresponds to the last digit of the stability constant.

^bProtonation constants reported in other media are provided for comparison. ^cRef 3, 0.1 M KCl, 25 °C. ^dRef 8, 0.1 M KCl, 25 °C. ^eRef 9, 0.1 M NaCl, 25 °C. ^fRef 10, 0.15 M NaCl, 25 °C.

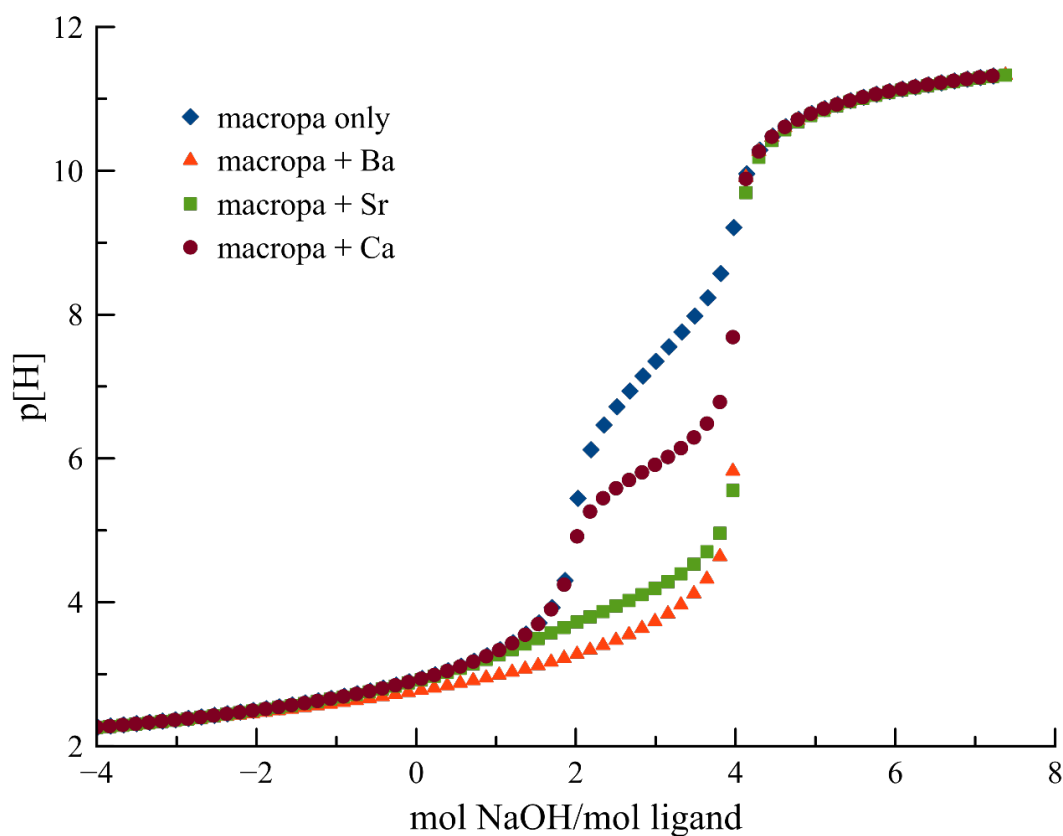


Figure S2. Overlay of potentiometric titration curves of macropa (1 mM) in the absence and presence of 1 equiv of Ca²⁺, Sr²⁺, or Ba²⁺. I = 0.2 M NaCl, 25 °C.

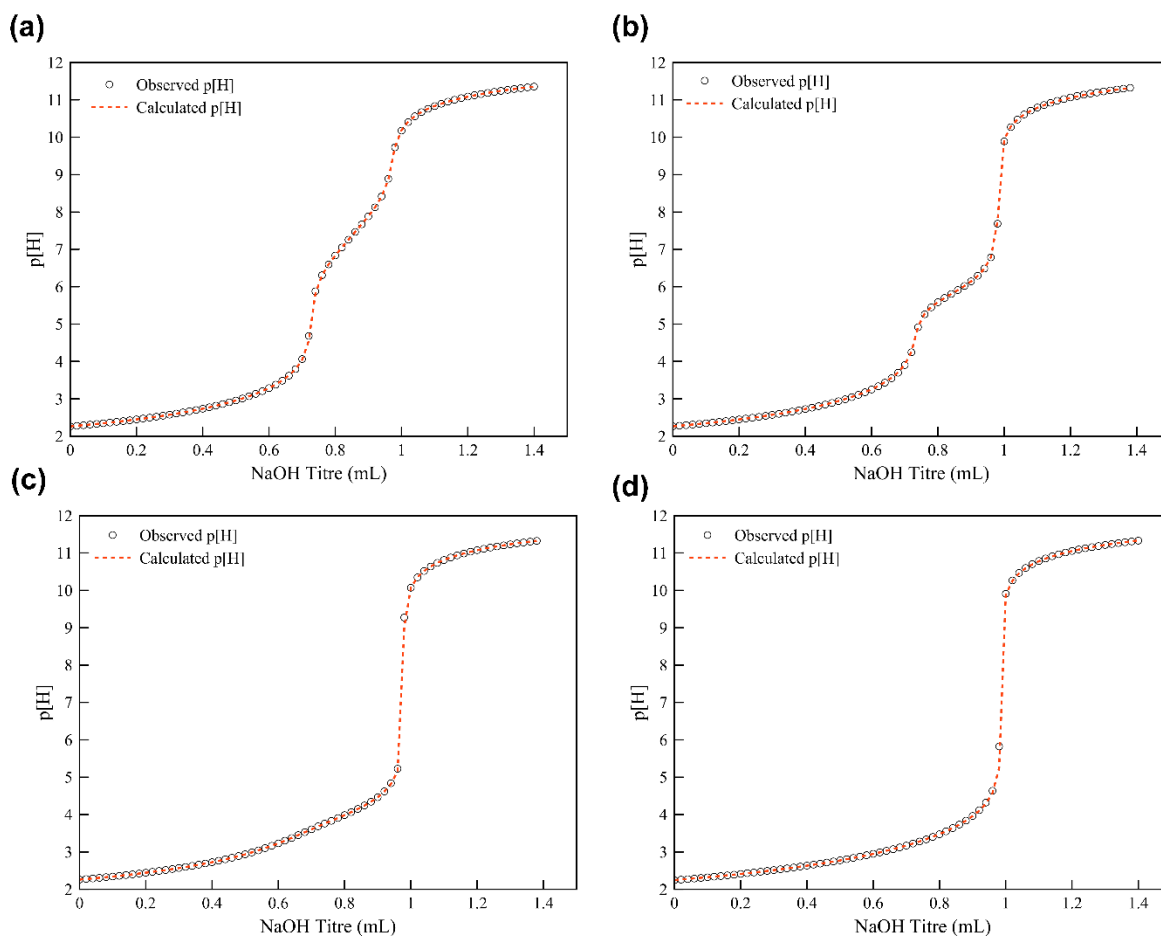


Figure S3. Representative potentiometric titrations of macropa (1 mM) in the (a) absence or presence of equimolar (b) Ca²⁺, (c) Sr²⁺, or (d) Ba²⁺, showing best-fit pH values calculated by Hyperquad. I = 0.2 M NaCl, 25 °C. Sigma values of the refinements were 0.370, 0.785, 0.311, and 0.643, respectively.

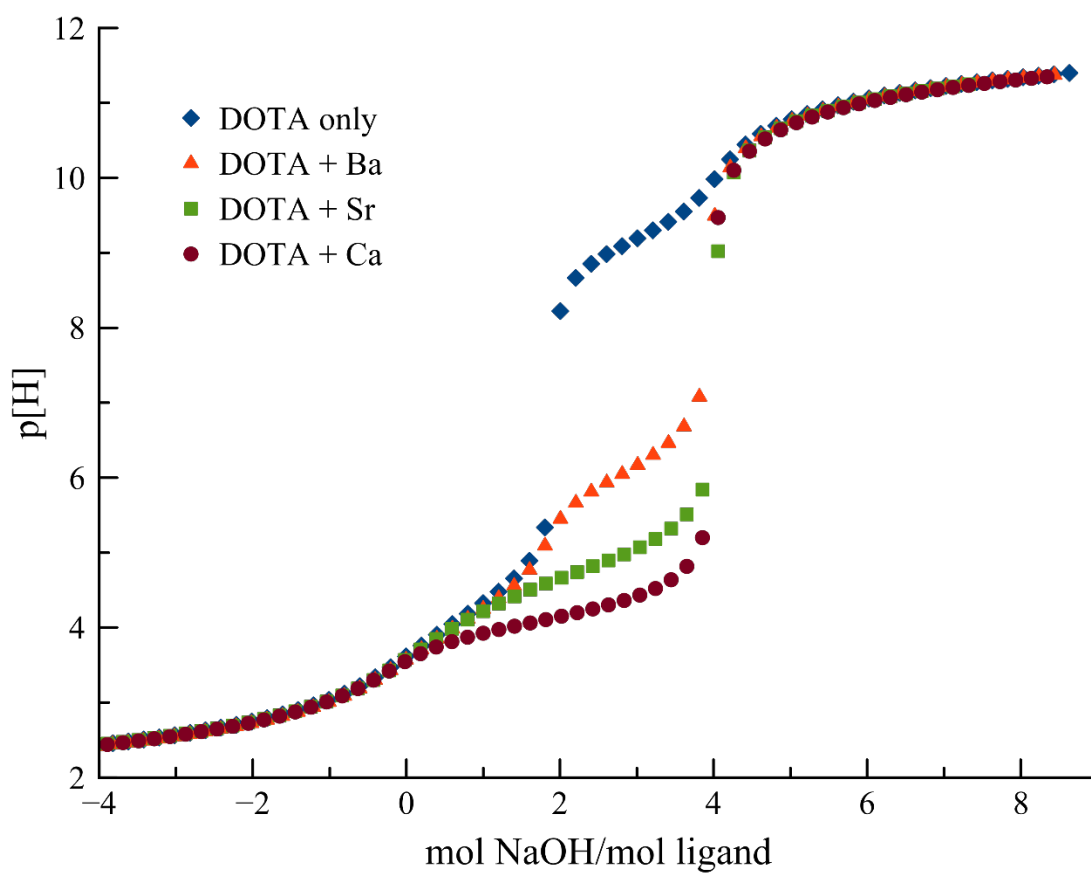


Figure S4. Overlay of potentiometric titration curves of DOTA (1 mM) in the absence and presence of 1 equiv of Ca^{2+} , Sr^{2+} , or Ba^{2+} . $I = 0.2 \text{ M NaCl}$, $25 \text{ }^\circ\text{C}$.

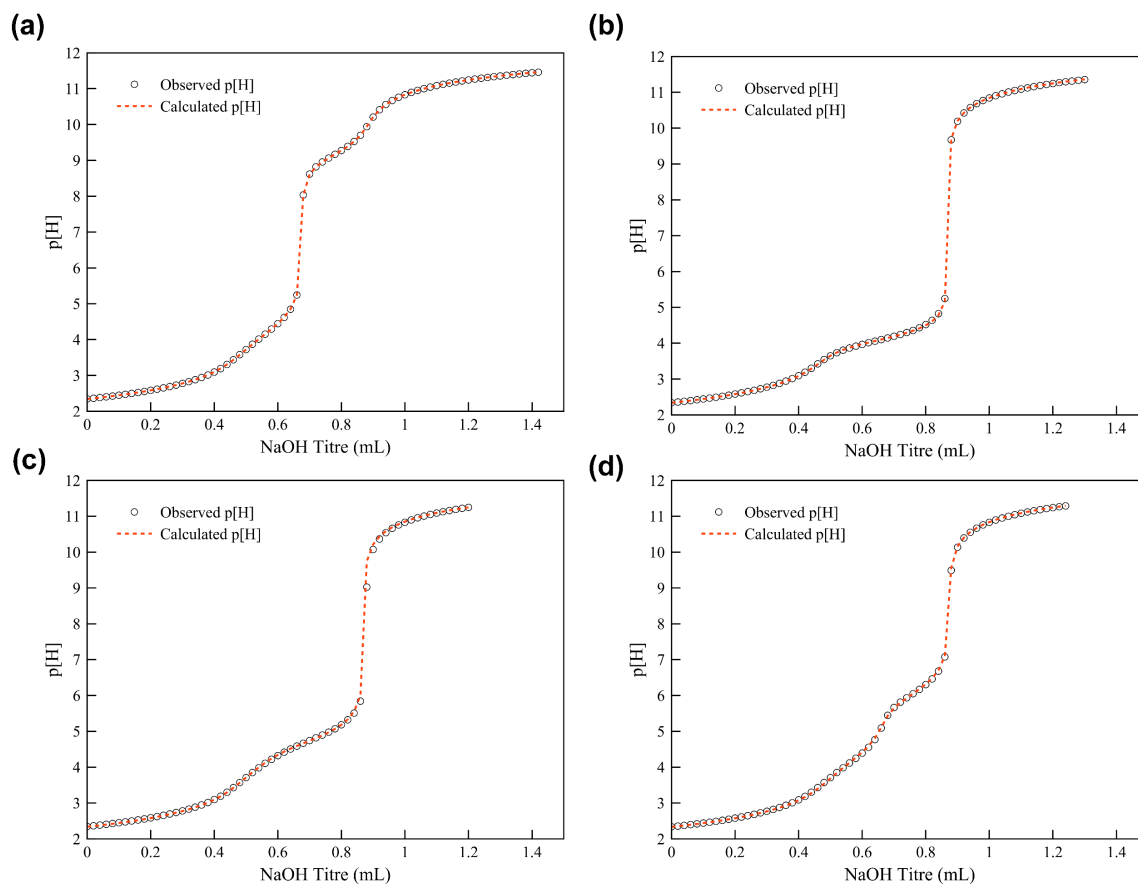


Figure S5. Representative potentiometric titrations of DOTA (1 mM) in the (a) absence or presence of equimolar (b) Ca^{2+} , (c) Sr^{2+} , or (d) Ba^{2+} , showing best-fit pH values calculated by Hyperquad. $I = 0.2 \text{ M NaCl}$, $25 \text{ }^\circ\text{C}$. Sigma values of the refinements were 0.260, 0.750, 1.280, and 0.846, respectively.

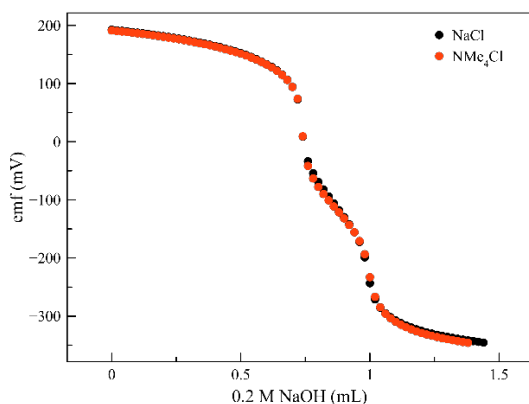


Figure S6. Overlay of potentiometric titration curves of macropa (1 mM) in 0.2 M NaCl or NMe₄Cl. Both titrations were carried out using 0.2 M NaOH as the base. The titration curves are nearly identical, indicating that macropa possesses negligible affinity for the Na^+ ion. This lack of affinity is expected on the basis of macropa's unique reverse-size selectivity for large over small metal ions.

2.1.3 Cation exchange method (^{223}Ra and ^{133}Ba)

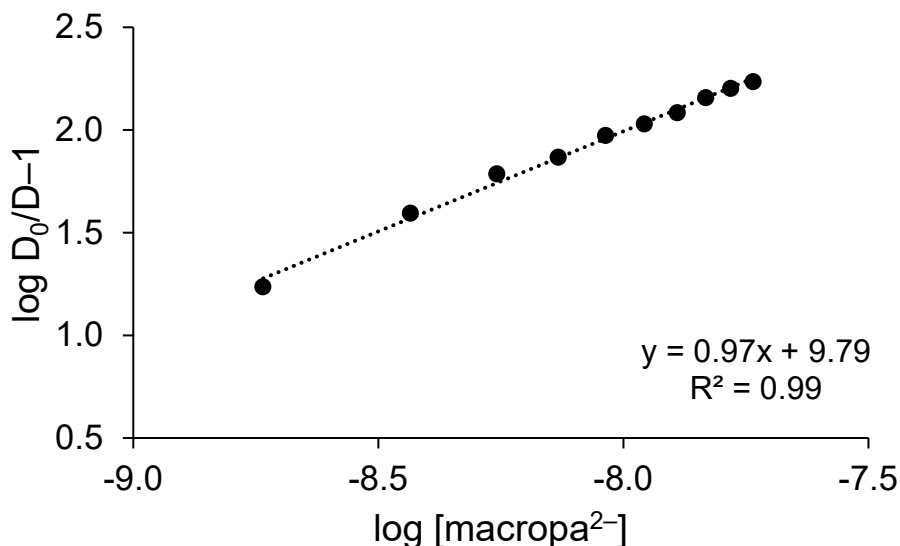


Figure S7. Representative determination of the stoichiometry of the complex formed between Ra^{2+} and macropa from distribution data at $\text{p}[\text{H}]$ 5.62. A ligand-to-metal stoichiometry of 0.97 is provided by the slope of the linear regression analysis of $\log D_0/D-1$ as a function of $\log [\text{macropa}^{2-}]$.

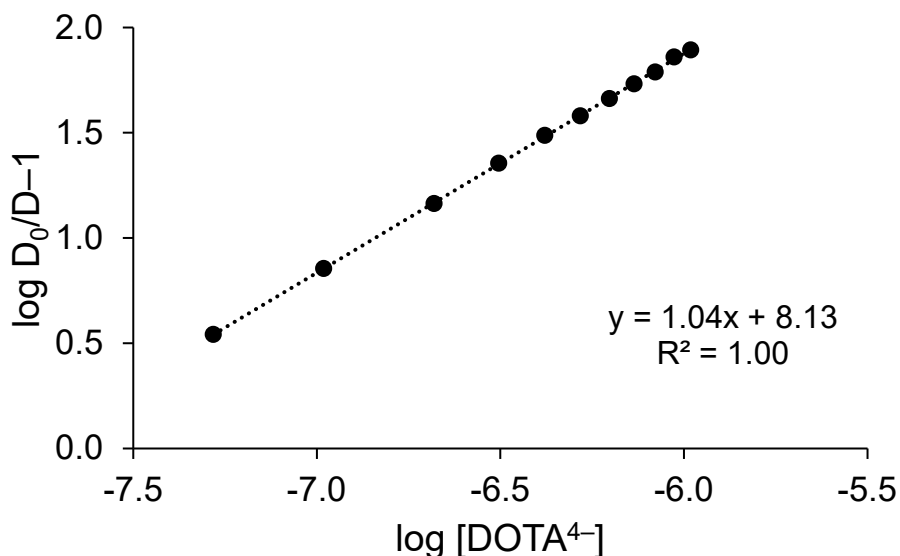


Figure S8. Representative determination of the stoichiometry of the complex formed between Ra^{2+} and DOTA from distribution data at $\text{p}[\text{H}]$ 7.68. A ligand-to-metal stoichiometry of 1.04 is provided by the slope of the linear regression analysis of $\log D_0/D-1$ as a function of $\log [\text{DOTA}^{4-}]$.

Table S2. Summary of distribution ratios and ^{223}Ra complex stoichiometry obtained from cation exchange experiments with varying concentrations of macropa at p[H] 5.62, 5.92, and 6.29.

p[H]	[Ligand] _{total} , M	D _{Ra}	L:Ra stoichiometry
5.62	0.0995– 5.97×10^{-5}	41.30–0.68	0.97 ± 0.03
5.92	0.0796– 3.84×10^{-5}	20.13–0.25	1.11 ± 0.05
6.29	0.398– 7.96×10^{-6}	65.03–0.25	1.25 ± 0.17

Table S3. Summary of distribution ratios and ^{223}Ra complex stoichiometry obtained from cation exchange experiments with varying concentrations of DOTA at p[H] 7.68, 8.07, and 8.46.

p[H]	[Ligand] _{total} , M	D _{Ra}	L:Ra stoichiometry
7.68	0.495– 9.90×10^{-4}	14.46–1.38	1.06 ± 0.02
8.07	0.354– 7.07×10^{-4}	10.21–0.40	1.11 ± 0.01
8.46	0.495– 4.95×10^{-4}	1.66–0.10	1.19 ± 0.02

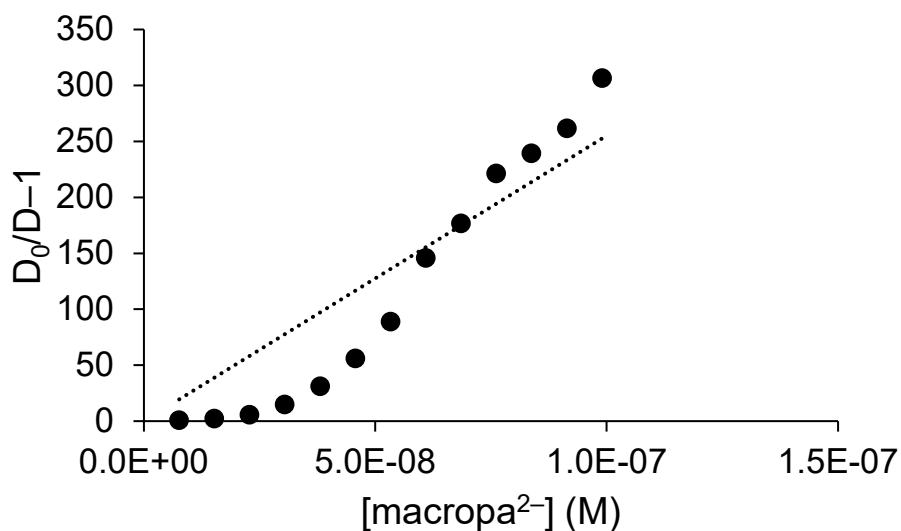


Figure S9. Determination of β_{app} for [Ra(macropa)] from distribution data at pH 12.4 and I = 0.2 M NaOH/Cl. Under these conditions, the plot of $D_0/D-1$ versus free macropa concentration did not yield the expected linear fit. We attribute this nonlinear trend to the presence of trace metal contaminants in solution, which compete with Ra^{2+} ions for binding to the ligand (see Section 1.5.3).

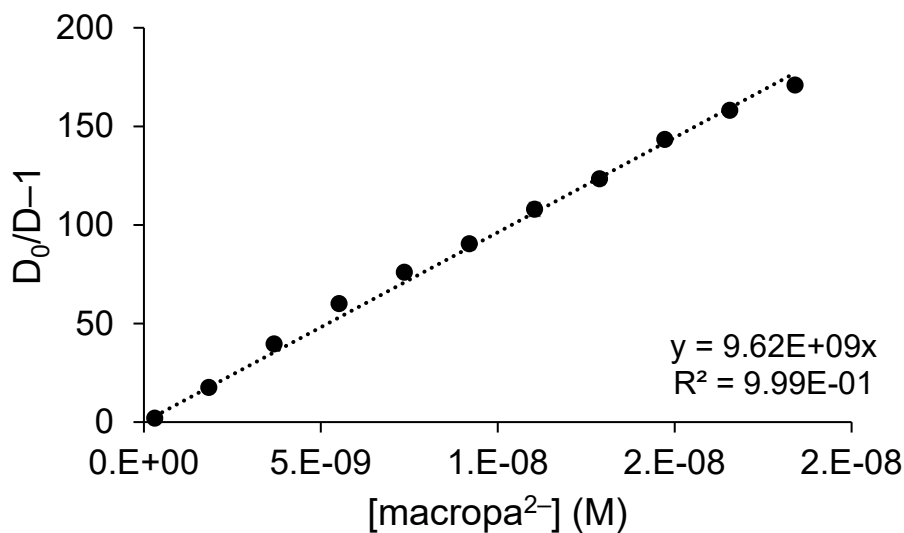


Figure S10. Determination of β_{app} for the Ra^{2+} complex of macropa from distribution data at p[H] 5.62. The data represents the average of three replicates. Error bars are shown when the uncertainty is larger than the symbol in the plot. The value for $\log \beta_{\text{app}}$ provided by the slope of the linear fit is 9.98.

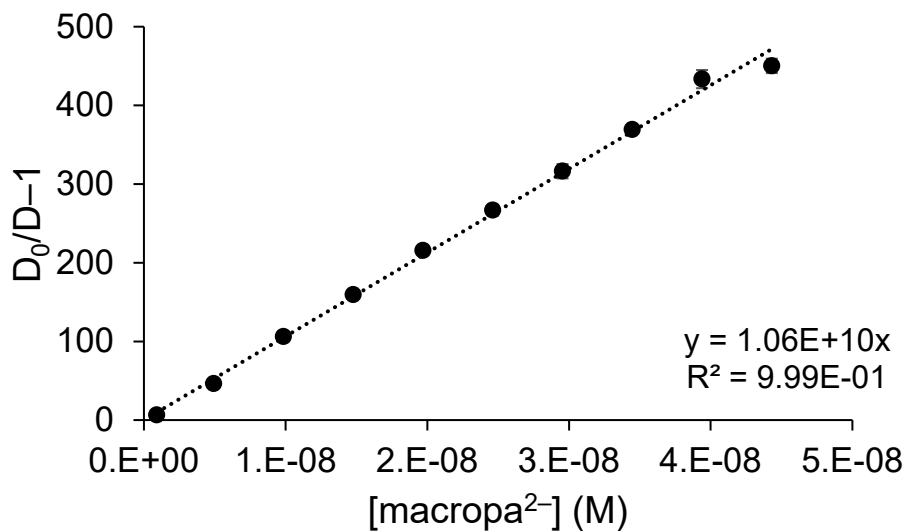


Figure S11. Determination of β_{app} for the Ra^{2+} complex of macropa from distribution data at $\text{p}[\text{H}]$ 5.92. The data represents the average of three replicates. Error bars are shown when the uncertainty is larger than the symbol in the plot. The value for $\log \beta_{\text{app}}$ provided by the slope of the linear fit is 10.03.

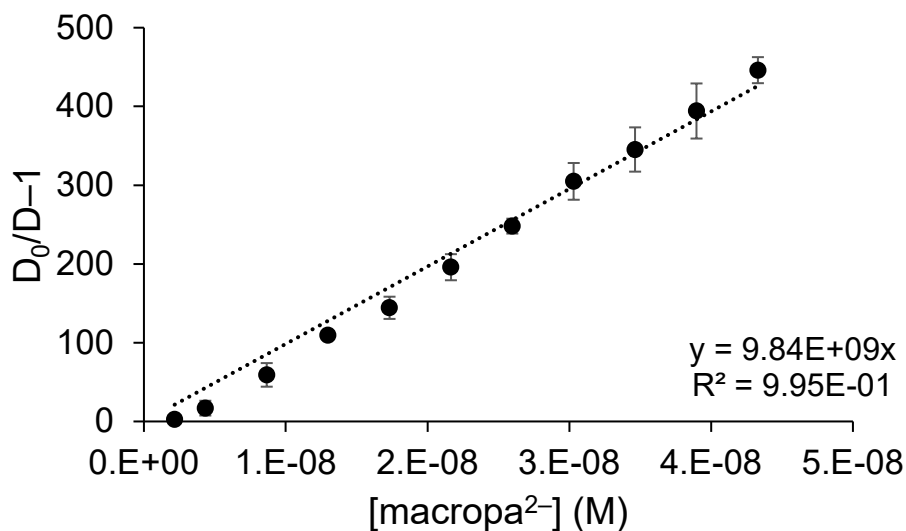


Figure S12. Determination of β_{app} for the Ra^{2+} complex of macropa from distribution data at $\text{p}[\text{H}]$ 6.29. The data represents the average of three replicates. Error bars are shown when the uncertainty is larger than the symbol in the plot. The value for $\log \beta_{\text{app}}$ provided by the slope of the linear fit is 9.99.

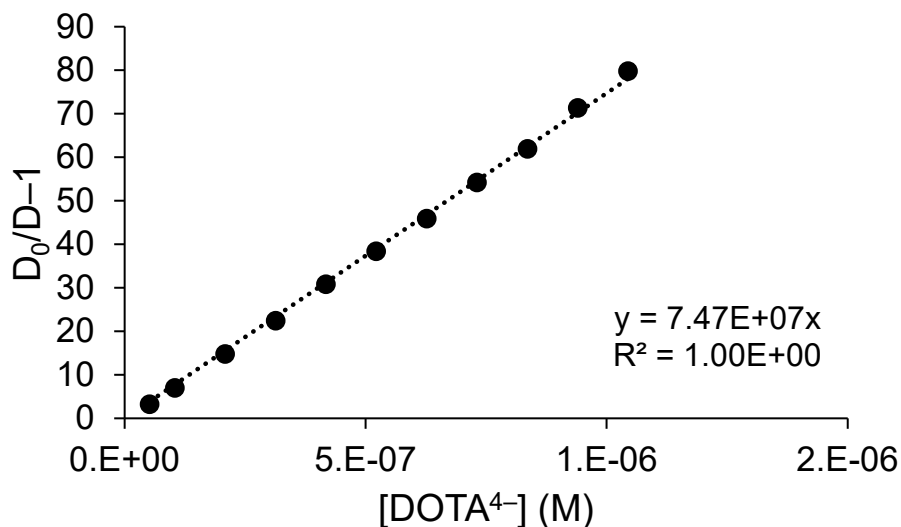


Figure S13. Determination of β_{app} for the Ra^{2+} complex of DOTA from distribution data at $\text{p}[\text{H}]$ 7.68. The data represents the average of three replicates. Error bars are shown when the uncertainty is larger than the symbol in the plot. The value for $\log \beta_{\text{app}}$ provided by the slope of the linear fit is 7.87.

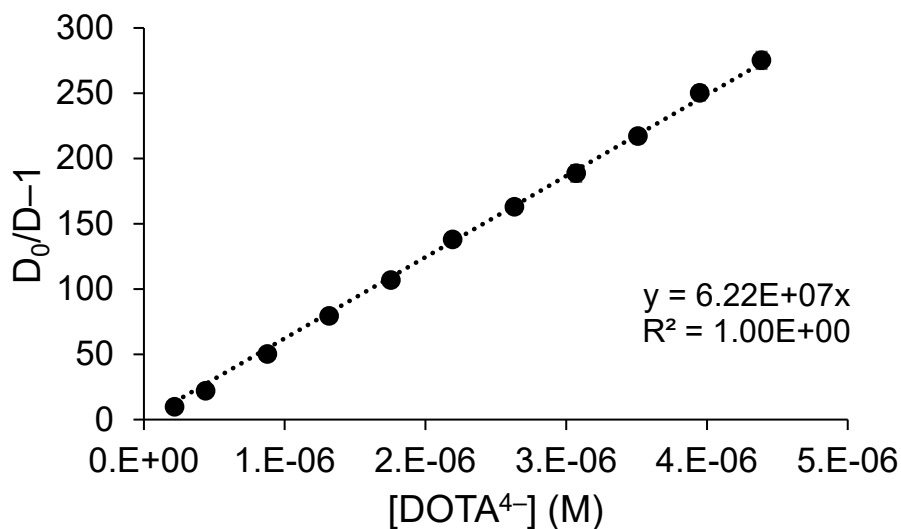


Figure S14. Determination of β_{app} for the Ra^{2+} complex of DOTA from distribution data at $\text{p}[\text{H}]$ 8.07. Error bars are shown when the uncertainty is larger than the symbol in the plot. The data represents the average of three replicates. The value for $\log \beta_{\text{app}}$ provided by the slope of the linear fit is 7.79.

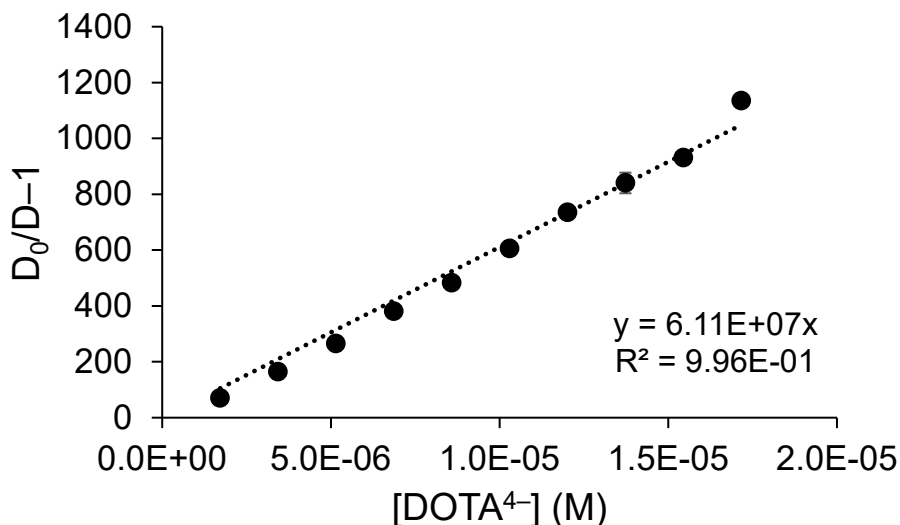


Figure S15. Determination of β_{app} for the Ra^{2+} complex of DOTA from distribution data at $p[H]$ 8.46. The data represents the average of three replicates. Error bars are shown when the uncertainty is larger than the symbol in the plot. The value for $\log \beta_{app}$ provided by the slope of the linear fit is 7.79.

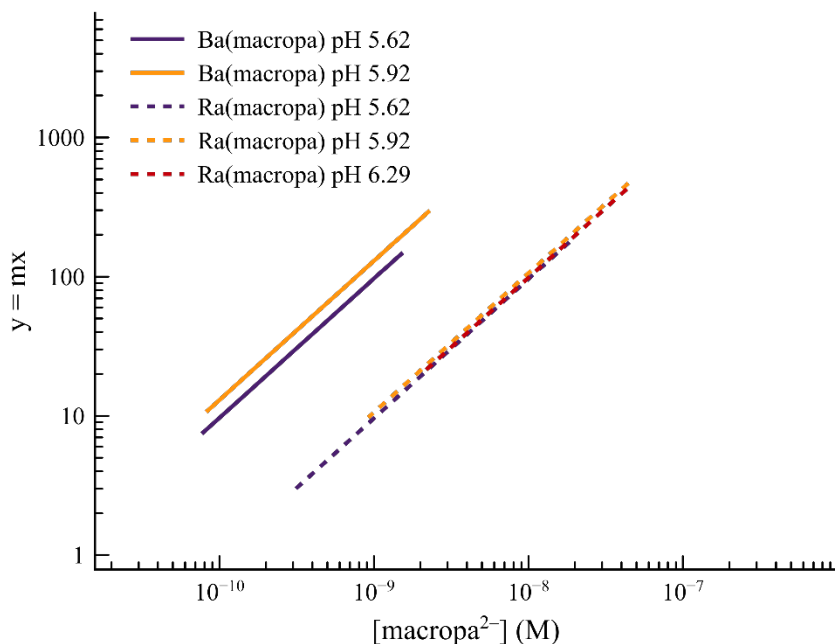


Figure S16. Variation in β_{app} of Ra^{2+} and Ba^{2+} complexes of macropa measured at different $p[H]$ values. Values of $D_0/D-1$ are plotted on the y-axis from the linear fit of the distribution data. The Ra^{2+} data overlap to form a single line, indicating that no protonated complexes form in aqueous solution from $p[H]$ 5.62 to 6.29. The lines formed from the Ba^{2+} data do not overlap. This lack of overlap is not due to the presence of protonated complexes within the $p[H]$ range of 5.62 and 5.92 because the β_{app} value of the Ba–macropa complex, provided by the y-intercept of the plot, is lower for the

data measured at p[H] 5.62 than at p[H] 5.92. The opposite trend would be expected if the variation in the two lines were due to the formation of protonated complexes. Rather, we attribute this lack of overlap to experimental error. Potential sources of error include differences in the resin batch used for each experiment and error associated with pH measurement of the buffers.

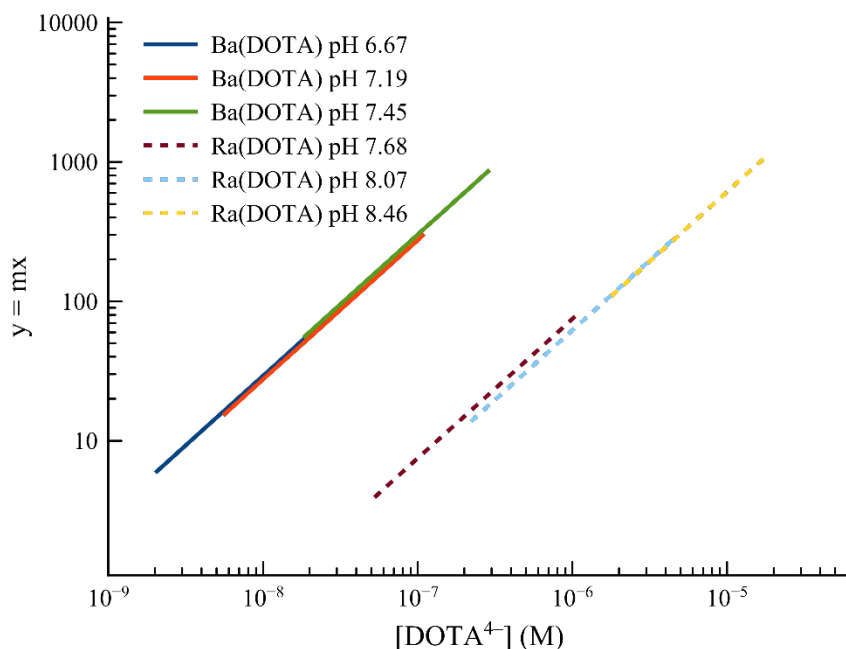


Figure S17. Variation in β_{app} of Ra^{2+} and Ba^{2+} complexes of DOTA measured at different p[H] values. Values of $D_0/D-1$ are plotted on the y-axis from the linear fit of the distribution data. The Ba^{2+} data overlap to form a single line, indicating that no protonated complexes form in aqueous solution from p[H] 6.67 to 7.45. Likewise, the linear fits from the Ra^{2+} data at p[H] 8.07 and p[H] 8.46 also overlap to form a single line. However, the line formed from the Ra^{2+} data at p[H] 7.68 is slightly shifted towards a higher y-intercept. Although the formation of protonated complexes in solution cannot be completely ruled out, we speculate that this small shift may be attributed to experimental error. This belief is based on the fact that the $\log \beta_{app}$ value measured at p[H] 6.67 differs from the values measured at p[H] 7.19 and p[H] 7.45 by only 0.08 log K units. This small difference is likely within the error of the method. Notably, excluding the data at p[H] 6.67 only negligibly changes our reported $\log K_{RaDOTA}$ value from 7.82 to 7.79. Therefore, we elect to present and include data from all three p[H] values in our calculation of $\log K_{RaDOTA}$.

Table S4. Summary of $\log \beta_{\text{app}}$ values for complexation of Ra^{2+} by DOTA or macropa as a function of solution p[H] . The values were obtained using distribution data from cation exchange experiments with ^{223}Ra . Each conditional constant represents the average of three replicates.

p[H]	DOTA	macropa
5.62	-	9.98(1)
5.92	-	10.03(1)
6.29	-	9.99(2)
7.68	7.87(1)	-
8.07	7.79(1)	-
8.46	7.79(1)	-
Average	7.82(4)	10.00(2)

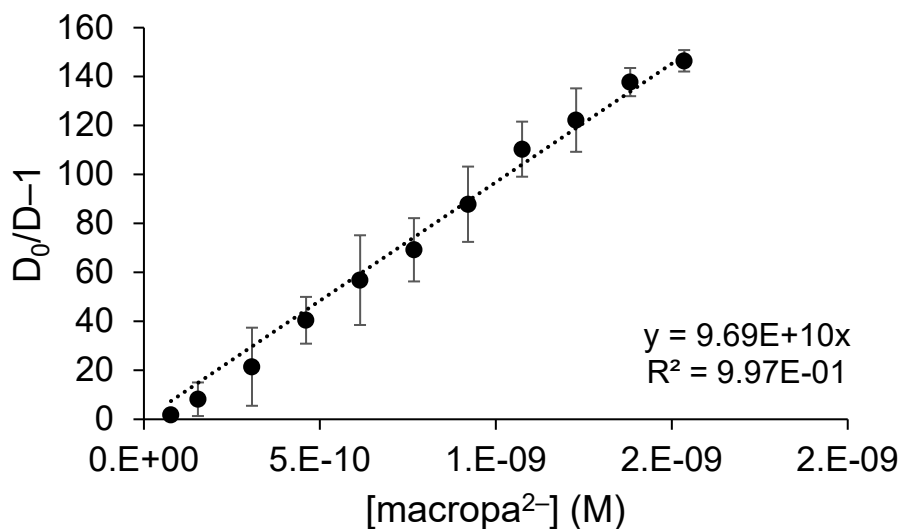


Figure S18. Determination of β_{app} for the Ba^{2+} complex of macropa from distribution data at p[H] 5.62. The data represents the average of three replicates. Error bars are shown when the uncertainty is larger than the symbol in the plot. The value for $\log \beta_{\text{app}}$ provided by the slope of the linear fit is 10.99.

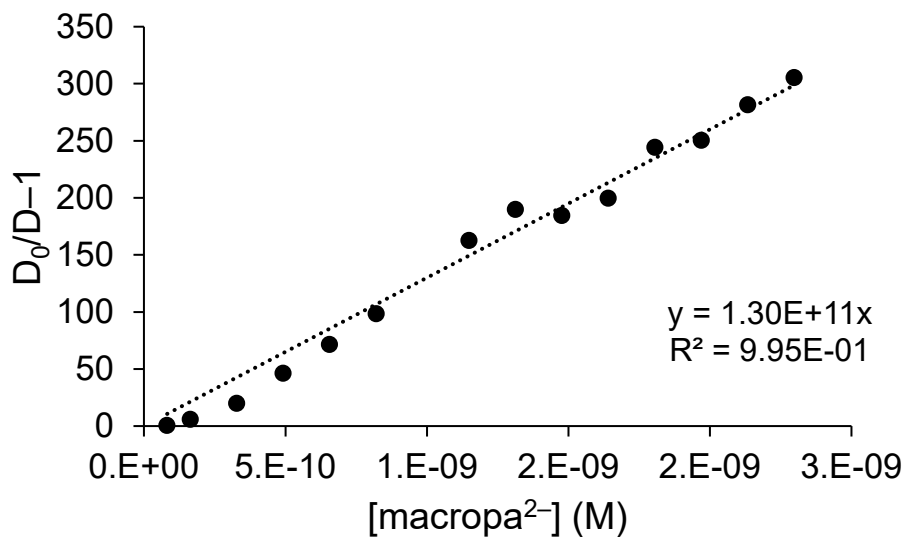


Figure S19. Determination of β_{app} for the Ba^{2+} complex of macropa from distribution data at $p[H]$ 5.92 ($n = 1$). The value for $\log \beta_{app}$ provided by the slope of the linear fit is 11.11.

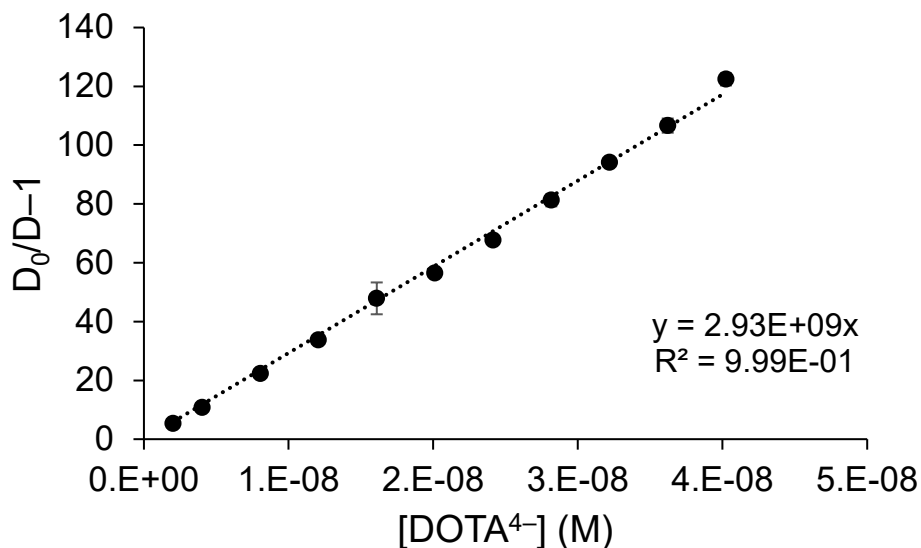


Figure S20. Determination of β_{app} for the Ba^{2+} complex of DOTA from distribution data at $p[H]$ 6.67 ($n = 3$). The value for $\log \beta_{app}$ provided by the slope of the linear fit is 9.47.

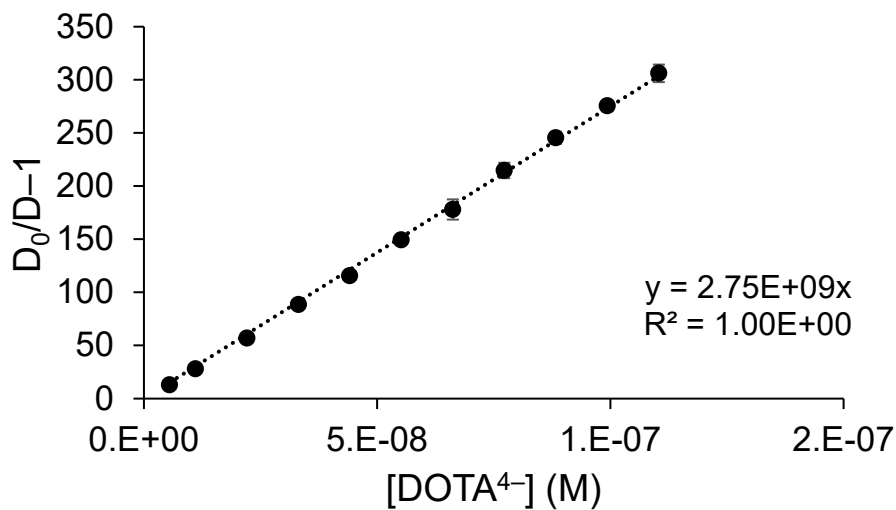


Figure S21. Determination of β_{app} for the Ba^{2+} complex of DOTA from distribution data at $\text{p}[\text{H}]$ 7.19 ($n = 5$). The value for $\log \beta_{\text{app}}$ provided by the slope of the linear fit is 9.44.

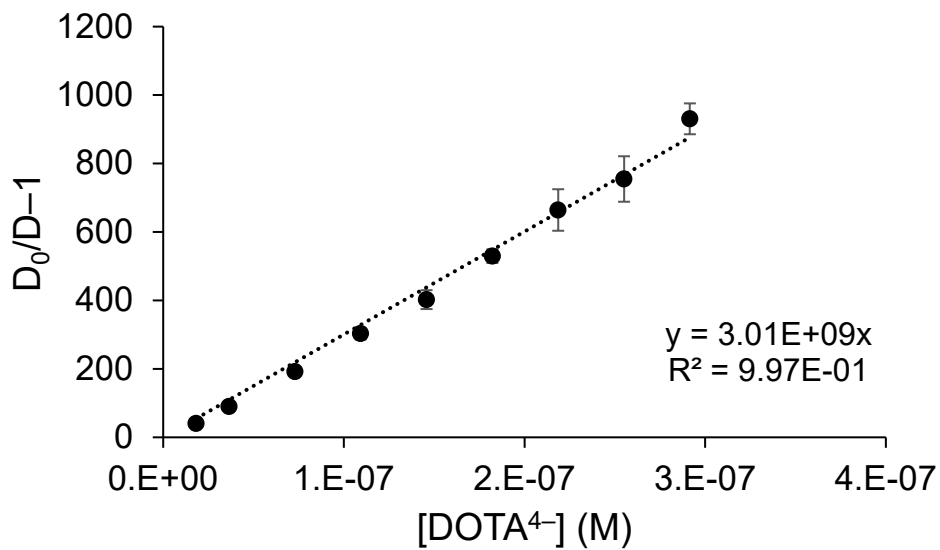


Figure S22. Determination of β_{app} for the Ba^{2+} complex of DOTA from distribution data at $\text{p}[\text{H}]$ 7.45 ($n = 3$). The value for $\log \beta_{\text{app}}$ provided by the slope of the linear fit is 9.48.

2.2 Density Functional Theory Calculations

Table S5. Comparison of experimental ($\Delta\Delta G^{\text{exp}}_{\text{aq}}$) and calculated ($\Delta\Delta G^{\text{calc}}_{\text{aq}}$) [B3LYP/SC/6-31+G* level of theory] Gibbs free energies (kcal/mol) for the reaction given by Equation (2) in the main text.

		Ca ²⁺ /Sr ²⁺	Ca ²⁺ /Ba ²⁺	Ca ²⁺ /Ra ²⁺
macropa	$\Delta\Delta G^{\text{exp}}_{\text{aq}}$	4.96	7.35	5.37
	$\Delta\Delta G^{\text{calc}}_{\text{aq}}$	6.82	9.36	6.60
DOTA	$\Delta\Delta G^{\text{exp}}_{\text{aq}}$	-2.55	-5.96	-7.99
	$\Delta\Delta G^{\text{calc}}_{\text{aq}}$	-1.94	-4.30	-7.94

Table S6. Wiberg bond indices of AE–ligand bonds in the studied complexes at the B3LYP/SC/def2TZVPP level.

Complex	AE–O _{carboxyl}	AE–N _{pyridine}	AE–O _{ether}	AE–N _{amine}
Ca–macropa	0.0511	0.0285	0.0224	0.0156
Sr–macropa	0.0430	0.0306	0.0217	0.0164
Ba–macropa	0.0453	0.0277	0.02045	0.0135
Ra–macropa	0.0432	0.0306	0.0199	0.0133

Complex	AE–O _{carboxyl}	AE–N _{amine}
Ca–DOTA	0.0557	0.0217
Sr–DOTA	0.0448	0.0176
Ba–DOTA	0.0406	0.0186
Ra–DOTA	0.0378	0.0181

Table S7. Leading donor-acceptor NBO interactions and their second-order stabilization energies $E^{(2)}$ (kcal/mol) for the macropa and DOTA complexes with the alkaline-earth (AE) metal ions at the B3LYP/SC/def2TZVPP level. LP = lone pair. n^*_{AE} = vacant valence orbitals of AE²⁺ metal ion. O, N, and AE represent oxygen, nitrogen, and metal ion, respectively.

Complex	Electron configuration	LP(O)→ n^*_{AE}	LP(N)→ n^*_{AE}	Total (kcal/mol)
Ca–macropa	4s(0.13)3d(0.07)5p(0.01)6d(0.01)	57.41	23.62	81.03
Sr–macropa	5s(0.13)4f(0.01)5d(0.05)6d(0.01)	55.19	29.49	84.68
Ba–macropa	6s(0.12)4f(0.02)5d(0.05)6d(0.01)	53.15	31.73	84.88
Ra–macropa	7s(0.13)5f(0.01)6d(0.03)7p(0.01)	49.18	28.69	77.87

Complex	Electron configuration	LP(O)→ n^*_{AE}	LP(N)→ n^*_{AE}	Total (kcal/mol)
Ca–DOTA	4s(0.12)3d(0.01)4p(0.01)5d(0.06)6d(0.01)	84.43	19.64	104.07
Sr–DOTA	5s(0.10)4d(0.01)5p(0.01)4f(0.01)5d(0.05)	61.86	18.99	80.85

Ba-DOTA	6s(0.08)4f(0.01)5d(0.01)6p(0.01)6d(0.05)7p(0.01)	51.62	15.41	67.03
Ra-DOTA	7s(0.08)5f(0.01)6d(0.01)7p(0.01)	40.25	14.92	55.17

Table S8. Calculated relative strain energies for neutral diaza-18-crown-6 and cyclen fragments of macropa and DOTA, respectively [relative to Ca-ligand, e.g., (strain energy of macropa in the Sr-macropa complex) – (strain energy of macropa in the Ca-macropa complex)].

Sr-macropa	Ba-macropa	Ra-macropa
0.04 kcal/mol	-1.04 kcal/mol	-1.36 kcal/mol

Sr-DOTA	Ba-DOTA	Ra-DOTA
0.21 kcal/mol	0.50 kcal/mol	0.75 kcal/mol

3. REFERENCES

- 1 X. Zeng, D. Coqui re, A. Alenda, E. Garrier, T. Prang , Y. Li, O. Reinaud and I. Jabin, *Chem. Eur. J.*, 2006, **12**, 6393–6402.
- 2 M. Mato-Iglesias, A. Roca-Sabio, Z. P link s, D. Esteban-G mez, C. Platas-Iglesias,  . T th, A. de Blas and T. Rodr guez-Blas, *Inorg. Chem.*, 2008, **47**, 7840–7851.
- 3 A. Roca-Sabio, M. Mato-Iglesias, D. Esteban-G mez,  . Toth, A. de Blas, C. Platas-Iglesias and T. Rodr guez-Blas, *J. Am. Chem. Soc.*, 2009, **131**, 3331–3341.
- 4 W. J. McDowell, P. T. Perdue and G. N. Case, *J. Inorg. Nucl. Chem.*, 1976, **38**, 2127–2129.
- 5 P. Gans and B. O’Sullivan, *Talanta*, 2000, **51**, 33–37.
- 6 H. S. Harned and B. B. Owen, *The Physical Chemistry of Electrolytic Solutions*, Reinhold Publishing Corp, New York, 3rd ed., 1958.
- 7 P. Gans, A. Sabatini and A. Vacca, *Talanta*, 1996, **43**, 1739–1753.
- 8 N. A. Thiele, S. N. MacMillan and J. J. Wilson, *J. Am. Chem. Soc.*, 2018, **140**, 17071–17078.
- 9 K. Kumar, C. A. Chang, L. C. Francesconi, D. D. Dischino, M. F. Malley, J. Z. Gougoutas and M. F. Tweedle, *Inorg. Chem.*, 1994, **33**, 3567–3575.
- 10 Z. Baranyai, Z. P link s, F. Uggeri and E. Br cher, *Eur. J. Inorg. Chem.*, 2010, 1948–1956.
- 11 G. Anderegg, F. Arnaud-Neu, R. Delgado, J. Felcman and K. Popov, *Pure Appl. Chem.*, 2005, **77**, 1445–1495.
- 12 R. Delgado and J. J. R. Fra sto Da Silva, *Talanta*, 1982, **29**, 815–822.
- 13 C. F. Baes and R. E. Mesmer, *The Hydrolysis of Cations*, Wiley, New York, 1976.
- 14 R. Ferreir s-Mart nez, D. Esteban-G mez,  . T th, A. de Blas, C. Platas-Iglesias and T. Rodr guez-Blas, *Inorg. Chem.*, 2011, **50**, 3772–3784.
- 15 D. S. Abou, N. A. Thiele, N. T. Gutsche, A. Villmer, H. Zhang, J. J. Woods, K. E. Baidoo, F. E. Escorcia, J. J. Wilson and D. L. J. Thorek, *Chem. Sci.*, 2021, **12**, 3733–3742.
- 16 M. P. Jensen, R. Chiarizia, I. A. Shkrob, J. S. Ulicki, B. D. Spindler, D. J. Murphy, M. Hossain, A. Roca-Sabio, C. Platas-Iglesias, A. de Blas and T. Rodr guez-Blas, *Inorg. Chem.*, 2014, **53**, 6003–6012.
- 17 M. P. Jensen, R. Chiarizia, J. S. Ulicki, B. D. Spindler, D. J. Murphy, M. M. Hossain, A. Roca-Sabio, A. de Blas and T. Rodr guez-Blas, *Solvent Extr. Ion Exch.*, 2015, **33**, 329–

- 345.
- 18 J. Schubert, *J. Phys. Chem.*, 1948, **52**, 340–350.
- 19 A. V. Matyskin, N. L. Hansson, P. L. Brown and C. Ekberg, *J. Solution Chem.*, 2017, **46**, 1951–1969.
- 20 J. Schubert and J. W. Richter, *J. Phys. Chem.*, 1948, **52**, 350–357.
- 21 J. Schubert, E. R. Russell and L. S. Myers, *J. Biol. Chem.*, 1950, **185**, 387–398.
- 22 J. Schubert, *J. Am. Chem. Soc.*, 1954, **76**, 3442–3444.
- 23 L. Baetslé and E. Bengsch, *J. Chromatogr. A*, 1962, **8**, 265–273.
- 24 T. Sekine, Y. Kawashima, T. Unnai and M. Sakairi, *Bull. Chem. Soc. Jpn.*, 1968, **41**, 3013–3015.
- 25 K. L. Nash, *Radiochim. Acta*, 1991, **54**, 171–180.
- 26 S. M. Shanbhag and G. R. Choppin, *Inorg. Chem.*, 1982, **21**, 1696–1697.
- 27 M. J. Frisch, G. W. Trucks, H. B. Schlegel, G. E. Scuseria, M. A. Robb, J. R. Cheeseman, G. Scalmani, V. Barone, G. A. Petersson, H. Nakatsuji, X. Li, M. Caricato, A. V. Marenich, J. Bloino, B. G. Janesko, R. Gomperts, B. Mennucci, H. P. Hratchian, J. V. Ortiz, A. F. Izmaylov, J. L. Sonnenberg, D. Williams-Young, F. Ding, F. Lipparini, F. Egidi, J. Goings, B. Peng, A. Petrone, T. Henderson, D. Ranasinghe, V. G. Zakrzewski, J. Gao, N. Rega, G. Zheng, W. Liang, M. Hada, M. Ehara, K. Toyota, R. Fukuda, J. Hasegawa, M. Ishida, T. Nakajima, Y. Honda, O. Kitao, H. Nakai, T. Vreven, K. Throssell, J. A. Montgomery, Jr., J. E. Peralta, F. Ogliaro, M. J. Bearpark, J. J. Heyd, E. N. Brothers, K. N. Kudin, V. N. Staroverov, T. A. Keith, R. Kobayashi, J. Normand, K. Raghavachari, A. P. Rendell, J. C. Burant, S. S. Iyengar, J. Tomasi, M. Cossi, J. M. Millam, M. Klene, C. Adamo, R. Cammi, J. W. Ochterski, R. L. Martin, K. Morokuma, O. Farkas, J. B. Foresman, and D. J. Fox, Gaussian 16, Revision A.03, Gaussian, Inc., Wallingford CT, 2016.
- 28 C. Lee, W. Yang and R. G. Parr, *Phys. Rev. B*, 1988, **37**, 785–789.
- 29 A. D. Becke, *J. Chem. Phys.*, 1993, **98**, 5648–5652.
- 30 I. S. Lim, H. Stoll and P. Schwerdtfeger, *J. Chem. Phys.*, 2006, **124**, 034107.
- 31 D. A. McQuarrie and J. D. Simon, *Molecular Thermodynamics*, University Science Books, 1999.
- 32 R. F. Ribeiro, A. V Marenich, C. J. Cramer and D. G. Truhlar, *J. Phys. Chem. B*, 2011, **115**, 14556–14562.
- 33 A. K. Rappé, C. J. Casewit, K. S. Colwell, W. A. Goddard III and W. M. Skiff, *J. Am.*

- Chem. Soc.*, 1992, **114**, 10024–10035.
- 34 R. D. Shannon, *Acta Crystallogr. Sect. A*, 1976, **32**, 751–767.
- 35 M. Mantina, A. C. Chamberlin, R. Valero, C. J. Cramer and D. G. Truhlar, *J. Phys. Chem. A*, 2009, **113**, 5806–5812.
- 36 M. Regueiro-Figueroa, D. Esteban-Gómez, A. De Blas, T. Rodríguez-Blas and C. Platas-Iglesias, *Chem. Eur. J.*, 2014, **20**, 3974–3981.
- 37 A. Kovacs, *ACS Omega*, 2020, **5**, 26431–26440.
- 38 E. D. Glendening, C. R. Landis and F. Weinhold, *J. Comput. Chem.*, 2013, **34**, 1429–1437.
- 39 J. P. Foster and F. Weinhold, *J. Am. Chem. Soc.*, 1980, **102**, 7211–7218.
- 40 A. E. Reed, L. A. Curtiss and F. Weinhold, *Chem. Rev.*, 1988, **88**, 899–926.

4. APPENDICES

A. HPGe Gamma-Ray Spectra

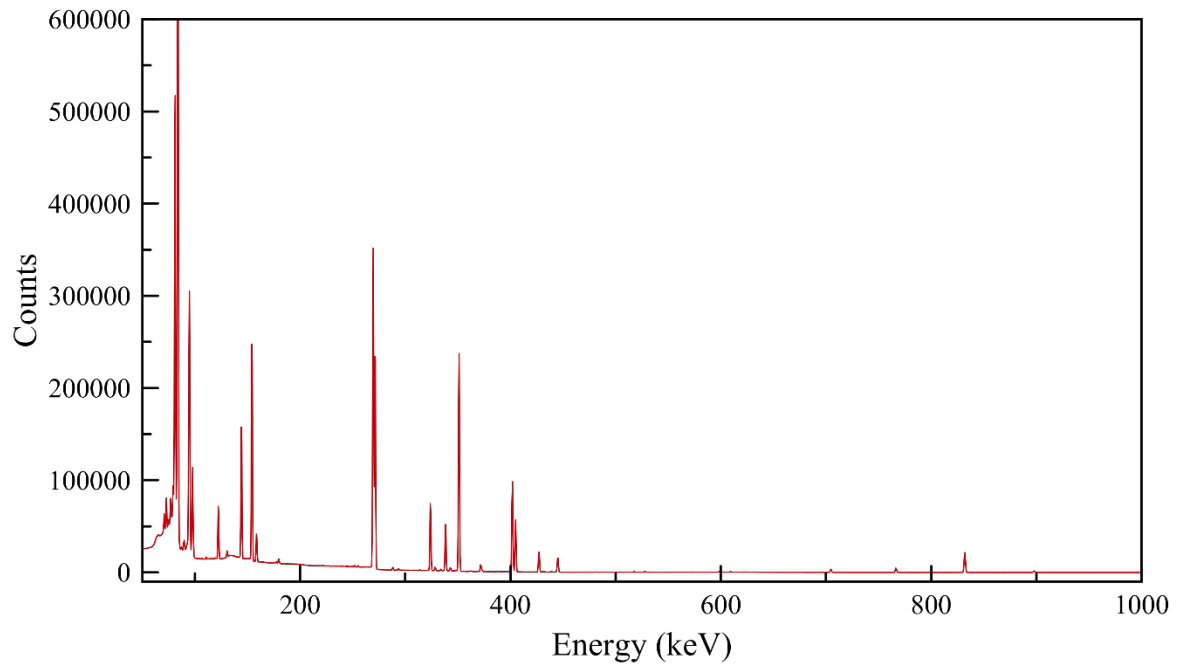
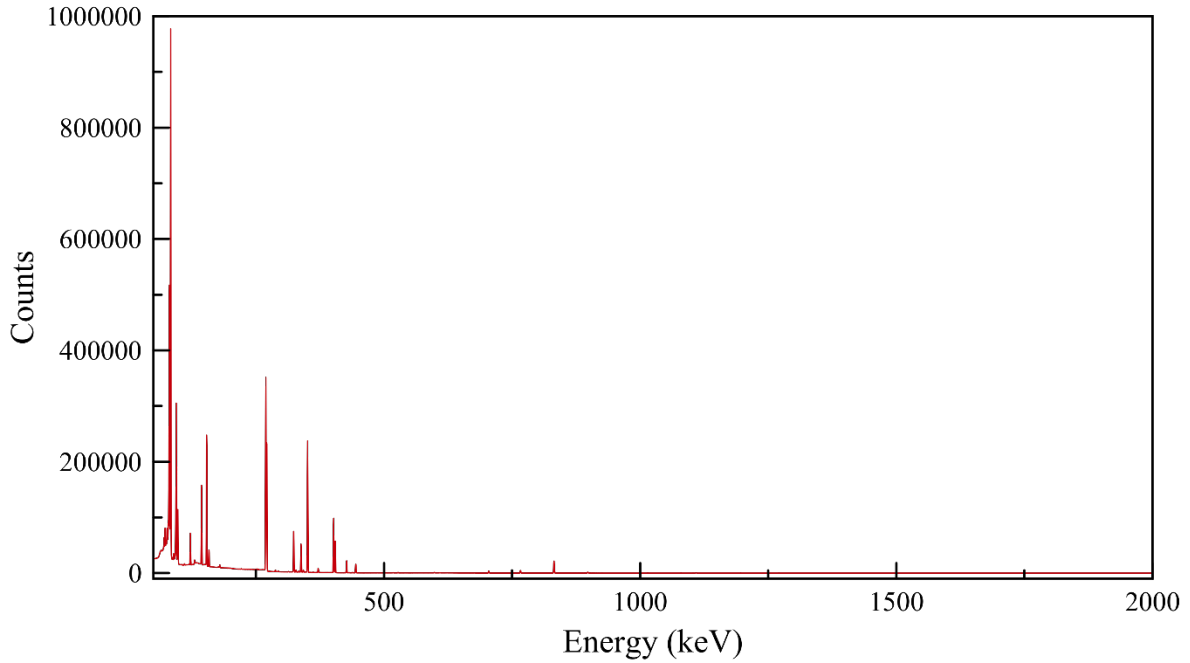


Figure A1. HPGe gamma-ray spectra of ^{223}Ra used in this work. Top: full view. Bottom: focused view.

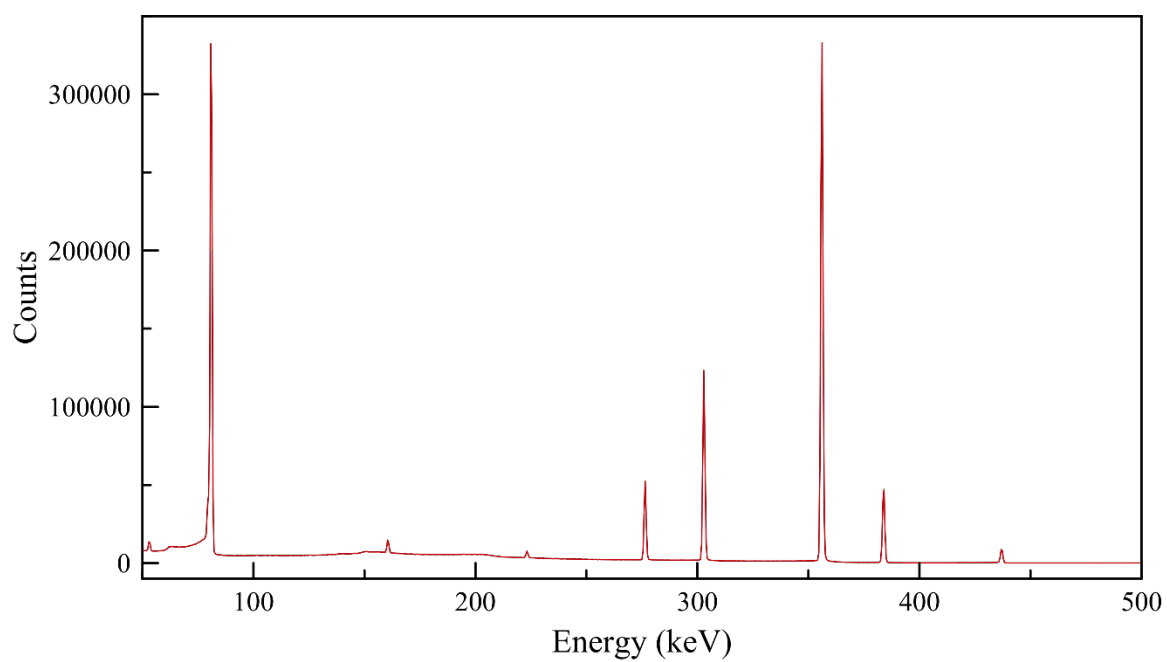
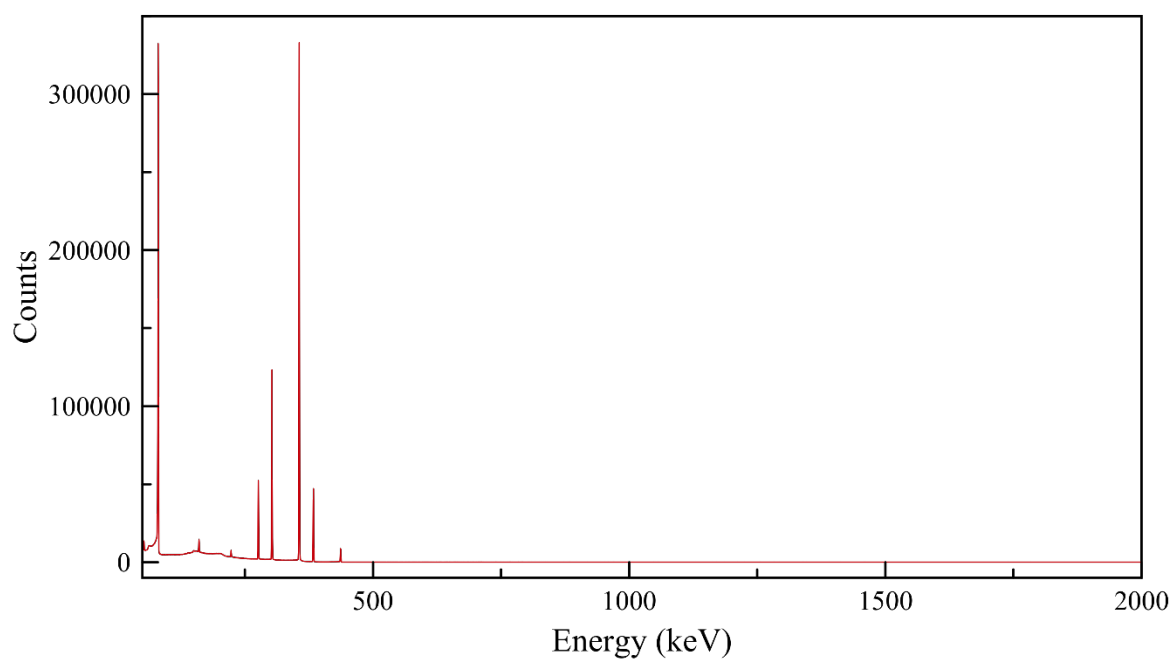


Figure A2. HPGe gamma-ray spectra of ^{133}Ba used in this work. Top: full view. Bottom: focused view.

B. Sample Gaussian 16 Input Files

Optimization {B3LYP/SC(Ra)/6-31+G*}

```
%mem=35GB
%NProcShared=32
#P B3LYP/gen gfinput pseudo=read scf=(MaxCycle=1000) integral=(grid=199302) opt=(maxcycle=999)
freq nosymm
```

Ra-nitrate_complex

```
0 1
N -0.0886 0.7902 3.0253
O -3.4948 0.5525 2.3159
O -2.8729 0.6724 -0.4697
O -0.9725 1.5601 2.5104
O 0.0476 0.6895 4.2402
O 3.2276 -0.5509 1.8846
O 2.2877 -2.3324 -0.1400
O 0.6471 0.1262 2.2162
H 3.9399 -0.5346 2.5415
H 2.3846 -0.3458 2.3549
H 2.7801 -1.9627 0.6216
H 2.7667 -2.0162 -0.9542
H -2.6644 1.0140 2.5917
H -4.1823 0.7874 2.9575
H -2.8841 1.5163 -0.9637
H -3.3553 0.8082 0.3687
N 0.0132 0.0737 -3.7379
O 3.3133 -1.0715 -2.3378
O -0.0562 -3.6270 -0.2884
O 0.6322 -0.9409 -3.2748
O 0.2897 0.5761 -4.8200
Ra -0.3143 -0.6977 -0.4554
O -1.9307 2.8503 -2.0677
O 0.0012 2.2984 -0.0790
O -0.9265 0.5489 -2.9964
H -2.2271 3.6069 -2.5956
H -1.5588 2.1820 -2.6962
H -0.6226 2.7626 -0.6768
H -0.3855 2.3077 0.8225
H 2.5980 -1.1093 -3.0041
H 3.1955 -0.1930 -1.9237
H 0.9240 -3.5495 -0.2307
H -0.2562 -4.4442 -0.7675
O 2.3369 0.8478 -0.4652
O -2.2459 -1.7710 1.4034
H 2.8199 0.6299 0.3579
H 1.8399 1.6748 -0.2984
H -2.1629 -2.5744 1.9378
H -2.8435 -1.1542 1.8800
```

```
H,N,O 0
6-31+G(d)
*****
Ra 0
S 6 1.00
212.70469 -0.000549
103.89397 0.003279
52.16554 -0.010178
26.45233 0.025662
13.23281 -0.058675
6.60443 0.102252
S 1 1.00
3.09818 1.0
S 1 1.00
1.43050 1.0
S 1 1.00
0.59710 1.0
S 1 1.00
0.25396 1.0
```

```

S 1 1.00
0.10987 1.0
S 1 1.00
0.04777 1.0
S 1 1.00
0.02061 1.0
! S 1 1.00
! 0.00933 1.0
! S 1 1.00
! 0.00407 1.0
P 5 1.00
85.15822 0.000620
43.00081 -0.002803
21.62348 0.008266
10.78370 -0.023706
5.34211 0.072636
P 1 1.00
2.47131 1.0
P 1 1.00
1.13910 1.0
P 1 1.00
0.41836 1.0
P 1 1.00
0.15633 1.0
P 1 1.00
0.07074 1.0
P 1 1.00
0.02932 1.0
! P 1 1.00
! 0.01266 1.0
! P 1 1.00
! 0.00563 1.0
! P 1 1.00
! 0.00268 1.0
D 1 1.00
3.09818 1.0
D 1 1.00
1.43050 1.0
D 1 1.00
0.59710 1.0
D 1 1.00
0.25396 1.0
D 1 1.00
0.10987 1.0
D 1 1.00
0.04777 1.0
! D 1 1.00
! 0.02061 1.0
! D 1 1.00
! 0.00933 1.0
! F 1 1.00
! 1.13910 1.0
! F 1 1.00
! 0.41836 1.0
! F 1 1.00
! 0.15633 1.0
! F 1 1.00
! 0.07074 1.0
! G 1 1.00
! 0.59710 1.0
! G 1 1.00
! 0.25396 1.0
! G 1 1.00
! 0.10987 1.0
****

```

```

Ra 0
ECP78MDF 5 78
H-Komponente
1
2 1. 0.

```

```

S-H
2
2 4.050730190 84.553966136
2 2.183125393 16.570871174
P-H
4
2 4.912257494 52.355105424
2 5.028625662 104.705297690
2 2.274507705 8.945169440
2 1.776652685 18.106864155
D-H
4
2 1.863529799 5.300115757
2 1.603971106 7.970570122
2 0.690407250 1.680466360
2 0.732716750 2.824510060
F-H
4
2 8.103105878 6.519691354
2 7.869446766 9.510581379
2 1.394055589 -2.922060062
2 1.337145152 -3.657363669
G-H
2
2 1.857939793 -5.335911193
2 1.821609586 -6.450124889

```

Optimization {B3LYP/SC(Ra)/def2TZVPP}

```

%mem=35GB
%NProcShared=32
#P B3LYP/gen gfinput pseudo=read scf=(MaxCycle=1000) integral=(grid=199302) opt=(maxcycle=999)
nosymm

```

Ra-nitrate_complex

```

0 1
N -0.0792 0.7595 3.0173
O -3.5127 0.5594 2.3331
O -2.8693 0.6750 -0.4676
O -0.9783 1.4901 2.4828
O 0.0669 0.7032 4.2258
O 3.2442 -0.5437 1.9117
O 2.3001 -2.3321 -0.1317
O 0.6614 0.0855 2.2265
H 3.9419 -0.5219 2.5736
H 2.3997 -0.3463 2.3697
H 2.7948 -1.9734 0.6244
H 2.7771 -2.0244 -0.9405
H -2.6824 1.0101 2.6037
H -4.1906 0.8026 2.9708
H -2.8862 1.5091 -0.9647
H -3.3596 0.8098 0.3583
N -0.0032 0.0637 -3.7132
O 3.3188 -1.0916 -2.3488
O -0.0541 -3.6009 -0.3279
O 0.6266 -0.9325 -3.2374
O 0.2355 0.5256 -4.8129
Ra -0.3053 -0.6770 -0.4333
O -1.9382 2.8600 -2.0889
O 0.0010 2.3250 -0.0774
O -0.9144 0.5639 -2.9584
H -2.2511 3.5931 -2.6271
H -1.5675 2.1869 -2.7030
H -0.6173 2.7851 -0.6724
H -0.3908 2.3248 0.8141
H 2.6025 -1.1257 -3.0046
H 3.2220 -0.2098 -1.9544
H 0.9185 -3.5253 -0.2520
H -0.2461 -4.4174 -0.7973

```

O	2.3550	0.8598	-0.4612
O	-2.2437	-1.7621	1.4144
H	2.8337	0.6482	0.3579
H	1.8662	1.6847	-0.3048
H	-2.2211	-2.5853	1.9106
H	-2.8551	-1.1553	1.8716

```

H,N,O 0
def2tzvpp
*****
Ra 0
S 6 1.00
212.70469 -0.000549
103.89397 0.003279
52.16554 -0.010178
26.45233 0.025662
13.23281 -0.058675
6.60443 0.102252
S 1 1.00
3.09818 1.0
S 1 1.00
1.43050 1.0
S 1 1.00
0.59710 1.0
S 1 1.00
0.25396 1.0
S 1 1.00
0.10987 1.0
S 1 1.00
0.04777 1.0
S 1 1.00
0.02061 1.0
S 1 1.00
0.00933 1.0
S 1 1.00
0.00407 1.0
P 5 1.00
85.15822 0.000620
43.00081 -0.002803
21.62348 0.008266
10.78370 -0.023706
5.34211 0.072636
P 1 1.00
2.47131 1.0
P 1 1.00
1.13910 1.0
P 1 1.00
0.41836 1.0
P 1 1.00
0.15633 1.0
P 1 1.00
0.07074 1.0
P 1 1.00
0.02932 1.0
P 1 1.00
0.01266 1.0
P 1 1.00
0.00563 1.0
P 1 1.00
0.00268 1.0
D 1 1.00
3.09818 1.0
D 1 1.00
1.43050 1.0
D 1 1.00
0.59710 1.0
D 1 1.00
0.25396 1.0
D 1 1.00
0.10987 1.0
D 1 1.00

```

0.04777 1.0
D 1 1.00
0.02061 1.0
D 1 1.00
0.00933 1.0
F 1 1.00
1.13910 1.0
F 1 1.00
0.41836 1.0
F 1 1.00
0.15633 1.0
F 1 1.00
0.07074 1.0
G 1 1.00
0.59710 1.0
G 1 1.00
0.25396 1.0
G 1 1.00
0.10987 1.0

Ra 0
ECP78MDF 5 78
H-Komponente
1
2 1. 0.
S-H
2
2 4.050730190 84.553966136
2 2.183125393 16.570871174
P-H
4
2 4.912257494 52.355105424
2 5.028625662 104.705297690
2 2.274507705 8.945169440
2 1.776652685 18.106864155
D-H
4
2 1.863529799 5.300115757
2 1.603971106 7.970570122
2 0.690407250 1.680466360
2 0.732716750 2.824510060
F-H
4
2 8.103105878 6.519691354
2 7.869446766 9.510581379
2 1.394055589 -2.922060062
2 1.337145152 -3.657363669
G-H
2
2 1.857939793 -5.335911193
2 1.821609586 -6.450124889

Solvation calculations {B3LYP/SC(Ra)/6-31+G*//IEF-PCM}

%mem=35GB
%NProcShared=32
#P B3LYP/gen ginput pseudo=read scf=(MaxCycle=1000) integral=(grid=199302)
scrf=(iefpcm,solvent=water,Read) nosymm

Ra-nitrate_complex-solvation

0 1
N -0.0886 0.7902 3.0253
O -3.4948 0.5525 2.3159
O -2.8729 0.6724 -0.4697
O -0.9725 1.5601 2.5104
O 0.0476 0.6895 4.2402
O 3.2276 -0.5509 1.8846
O 2.2877 -2.3324 -0.1400

O	0.6471	0.1262	2.2162
H	3.9399	-0.5346	2.5415
H	2.3846	-0.3458	2.3549
H	2.7801	-1.9627	0.6216
H	2.7667	-2.0162	-0.9542
H	-2.6644	1.0140	2.5917
H	-4.1823	0.7874	2.9575
H	-2.8841	1.5163	-0.9637
H	-3.3553	0.8082	0.3687
N	0.0132	0.0737	-3.7379
O	3.3133	-1.0715	-2.3378
O	-0.0562	-3.6270	-0.2884
O	0.6322	-0.9409	-3.2748
O	0.2897	0.5761	-4.8200
Ra	-0.3143	-0.6977	-0.4554
O	-1.9307	2.8503	-2.0677
O	0.0012	2.2984	-0.0790
O	-0.9265	0.5489	-2.9964
H	-2.2271	3.6069	-2.5956
H	-1.5588	2.1820	-2.6962
H	-0.6226	2.7626	-0.6768
H	-0.3855	2.3077	0.8225
H	2.5980	-1.1093	-3.0041
H	3.1955	-0.1930	-1.9237
H	0.9240	-3.5495	-0.2307
H	-0.2562	-4.4442	-0.7675
O	2.3369	0.8478	-0.4652
O	-2.2459	-1.7710	1.4034
H	2.8199	0.6299	0.3579
H	1.8399	1.6748	-0.2984
H	-2.1629	-2.5744	1.9378
H	-2.8435	-1.1542	1.8800

H,N,O 0
6-31+G(d)

Ra 0
S 6 1.00
212.70469 -0.000549
103.89397 0.003279
52.16554 -0.010178
26.45233 0.025662
13.23281 -0.058675
6.60443 0.102252
S 1 1.00
3.09818 1.0
S 1 1.00
1.43050 1.0
S 1 1.00
0.59710 1.0
S 1 1.00
0.25396 1.0
S 1 1.00
0.10987 1.0
S 1 1.00
0.04777 1.0
S 1 1.00
0.02061 1.0
! S 1 1.00
! 0.00933 1.0
! S 1 1.00
! 0.00407 1.0
P 5 1.00
85.15822 0.000620
43.00081 -0.002803
21.62348 0.008266
10.78370 -0.023706
5.34211 0.072636
P 1 1.00
2.47131 1.0
P 1 1.00

1.13910 1.0
 P 1 1.00
 0.41836 1.0
 P 1 1.00
 0.15633 1.0
 P 1 1.00
 0.07074 1.0
 P 1 1.00
 0.02932 1.0
 ! P 1 1.00
 ! 0.01266 1.0
 ! P 1 1.00
 ! 0.00563 1.0
 ! P 1 1.00
 ! 0.00268 1.0
 D 1 1.00
 3.09818 1.0
 D 1 1.00
 1.43050 1.0
 D 1 1.00
 0.59710 1.0
 D 1 1.00
 0.25396 1.0
 D 1 1.00
 0.10987 1.0
 D 1 1.00
 0.04777 1.0
 ! D 1 1.00
 ! 0.02061 1.0
 ! D 1 1.00
 ! 0.00933 1.0
 ! F 1 1.00
 ! 1.13910 1.0
 ! F 1 1.00
 ! 0.41836 1.0
 ! F 1 1.00
 ! 0.15633 1.0
 ! F 1 1.00
 ! 0.07074 1.0
 ! G 1 1.00
 ! 0.59710 1.0
 ! G 1 1.00
 ! 0.25396 1.0
 ! G 1 1.00
 ! 0.10987 1.0

Ra 0
 ECP78MDF 5 78
 H-Komponente
 1
 2 1. 0.
 S-H
 2
 2 4.050730190 84.553966136
 2 2.183125393 16.570871174
 P-H
 4
 2 4.912257494 52.355105424
 2 5.028625662 104.705297690
 2 2.274507705 8.945169440
 2 1.776652685 18.106864155
 D-H
 4
 2 1.863529799 5.300115757
 2 1.603971106 7.970570122
 2 0.690407250 1.680466360
 2 0.732716750 2.824510060
 F-H
 4
 2 8.103105878 6.519691354

```
2 7.869446766 9.510581379
2 1.394055589 -2.922060062
2 1.337145152 -3.657363669
G-H
2
2 1.857939793 -5.335911193
2 1.821609586 -6.450124889
```

ModifySph

Ra 2.512 1.0

C. Cartesian Coordinates

Optimized [Ra(macropa)] at the B3LYP/SC(Ra)/def2TZVPP level:

Ra	-0.000204000	-0.000249000	-0.191103000
O	-0.443219000	-2.493265000	-1.897660000
O	-2.488267000	-0.420406000	-1.979741000
O	0.441019000	2.491384000	-1.900648000
O	2.485941000	0.418613000	-1.982895000
O	-2.041244000	-0.993601000	1.270351000
O	-2.999961000	-2.310252000	2.823846000
O	2.043192000	0.996607000	1.264675000
O	3.002691000	2.310353000	2.820161000
N	2.206168000	-2.282013000	-0.612767000
N	-2.206920000	2.281545000	-0.612396000
N	0.328993000	-2.299330000	1.588591000
N	-0.326986000	2.301180000	1.586448000
C	1.629686000	-3.492852000	-1.210207000
H	1.061925000	-4.017380000	-0.444561000
H	2.413255000	-4.183904000	-1.559963000
C	0.682629000	-3.221771000	-2.369362000
H	1.171193000	-2.669298000	-3.181122000
H	0.355728000	-4.185820000	-2.777418000
C	-1.560328000	-2.489409000	-2.774440000
H	-1.842589000	-3.520096000	-3.021100000
H	-1.314378000	-1.969737000	-3.708965000
C	-2.730538000	-1.818622000	-2.093763000
H	-3.631837000	-1.989088000	-2.695952000
H	-2.886687000	-2.252838000	-1.101481000
C	-3.556727000	0.267364000	-1.316876000
H	-3.620978000	-0.079276000	-0.281840000
H	-4.501406000	0.033469000	-1.822757000
C	-3.322860000	1.763659000	-1.418522000
H	-3.124418000	1.991480000	-2.466033000
H	-4.260676000	2.277079000	-1.156299000
C	-1.631106000	3.491648000	-1.211965000
H	-1.062399000	4.017056000	-0.447625000
H	-2.415068000	4.182309000	-1.561601000
C	-0.685441000	3.219175000	-2.371917000
H	-1.174952000	2.665665000	-3.182415000
H	-0.359144000	4.182760000	-2.781570000
C	1.557266000	2.486905000	-2.778489000
H	1.839231000	3.517412000	-3.026245000
H	1.310465000	1.966460000	-3.712361000
C	2.728141000	1.816720000	-2.098352000
H	3.628858000	1.986653000	-2.701562000
H	2.885174000	2.251732000	-1.106564000
C	3.555371000	-0.268706000	-1.321202000
H	3.621464000	0.079006000	-0.286651000
H	4.499235000	-0.035540000	-1.828953000
C	3.320515000	-1.765066000	-1.420941000
H	3.121164000	-1.993938000	-2.467942000
H	4.259186000	-2.278367000	-1.159485000
C	2.621992000	-2.491229000	0.787229000
H	3.014101000	-1.540810000	1.157926000
H	3.438971000	-3.226590000	0.846302000
C	1.500992000	-2.928327000	1.710406000
C	1.696070000	-3.922571000	2.662949000
H	2.651836000	-4.422704000	2.744269000
C	0.639620000	-4.257208000	3.504325000
H	0.768005000	-5.022517000	4.259219000
C	-0.577561000	-3.613180000	3.355479000
H	-1.439735000	-3.842733000	3.963293000
C	-0.700542000	-2.631934000	2.373031000
C	-2.050262000	-1.915417000	2.149530000
C	-2.620960000	2.492379000	0.787896000
H	-3.012571000	1.542387000	1.160207000
H	-3.437845000	3.227824000	0.847179000
C	-1.498708000	2.930495000	1.709051000
C	-1.692397000	3.925988000	2.660589000
H	-2.647961000	4.426420000	2.742453000

C	-0.634855000	4.261410000	3.500263000
H	-0.762104000	5.027721000	4.254333000
C	0.581958000	3.616806000	3.350787000
H	1.444854000	3.846673000	3.957459000
C	0.703550000	2.634447000	2.369291000
C	2.052823000	1.917263000	2.145115000

Optimized [Ra(DOTA)]²⁻ at the B3LYP/SC(Ra)/def2TZVPP level:

Ra	3.205004000	3.205011000	1.612772000
O	5.596301000	1.818203000	1.936355000
O	7.824754000	1.619076000	1.654071000
N	5.378649000	2.809946000	-0.710255000
C	4.951741000	5.236283000	-1.257419000
H	5.647643000	5.531718000	-0.475378000
H	5.109178000	5.938783000	-2.098101000
C	5.316212000	3.835029000	-1.750855000
H	4.595843000	3.519718000	-2.505016000
H	6.285309000	3.911692000	-2.278444000
C	6.625846000	2.909663000	0.064572000
H	6.738294000	3.937839000	0.412216000
H	7.496840000	2.675562000	-0.566821000
C	6.694108000	2.015367000	1.340022000
O	4.591937000	5.596291000	1.936291000
O	4.790828000	7.824780000	1.654107000
N	3.600045000	5.378646000	-0.710253000
C	1.173711000	4.951741000	-1.257441000
H	0.878258000	5.647645000	-0.475409000
H	0.471219000	5.109165000	-2.098132000
C	2.574968000	5.316219000	-1.750862000
H	2.890285000	4.595855000	-2.505026000
H	2.498311000	6.285320000	-2.278444000
C	3.500328000	6.625841000	0.064578000
H	2.472150000	6.738292000	0.412218000
H	3.734432000	7.496835000	-0.566812000
C	4.394602000	6.694115000	1.340042000
O	1.818156000	0.813716000	1.936333000
O	1.619120000	-1.414750000	1.654093000
N	2.809946000	1.031354000	-0.710268000
C	5.236285000	1.458253000	-1.257428000
H	5.531720000	0.762342000	-0.475394000
H	5.938790000	1.300820000	-2.098107000
C	3.835032000	1.093785000	-1.750866000
H	3.519722000	1.814151000	-2.505031000
H	3.911695000	0.124685000	-2.278449000
C	2.909664000	-0.215831000	0.064574000
H	3.937841000	-0.328273000	0.412221000
H	2.675572000	-1.086836000	-0.566808000
C	2.015366000	-0.284095000	1.340021000
O	0.813726000	4.591984000	1.936268000
O	-1.414776000	4.790784000	1.654129000
N	1.031357000	3.600046000	-0.710266000
C	1.458253000	1.173709000	-1.257450000
H	0.762339000	0.878257000	-0.475425000
H	1.300833000	0.471213000	-2.098139000
C	1.093778000	2.574965000	-1.750872000
H	1.814139000	2.890280000	-2.505040000
H	0.124674000	2.498308000	-2.278450000
C	-0.215826000	3.500326000	0.064581000
H	-0.328271000	2.472148000	0.412223000
H	-1.086831000	3.734422000	-0.566799000
C	-0.284101000	4.394603000	1.340041000